

**River Discharge Estimation Using Multisource Remote Sensing:  
Application in the Lancang Mekong River Basin**

by

xxxxxxx

A Thesis Proposal Submitted in Partial Fulfillment of the Requirements for the  
Degree of  
Master of Engineering in Water Engineering and Management

Examination Committee: Prof. xxxxxx (Chairperson)  
Dr. S. xxxxxxxx (Member)  
Dr. xxxxxxx (Member)  
Dr. xxxxxxx (Member)

Nationality: xxxxxx

Previous Degree: Bachelor of Engineering in Agricultural Engineering  
Institute of Engineering  
xxxxxxx

Scholarship Donor: ADB-JSP Scholarship

Asian Institute of Technology  
School of Engineering and Technology  
Thailand  
September 2022

## **CONTENTS**

<b>LIST OF TABLES</b>	<b>iv</b>
<b>LIST OF FIGURES</b>	<b>v</b>
<b>LIST OF ABBREVIATIONS</b>	<b>vi</b>
<b>CHAPTER 1 INTRODUCTION</b>	<b>1</b>
1.1 Background of the Study	1
1.2 Statement of the Problem	3
1.3 Research Questions	4
1.4 Objectives of the Study	4
1.5 Scope and limitations of the Study	5
<b>CHAPTER 2 LITERATURE REVIEW</b>	<b>6</b>
2.1 Importance of Monitoring River Flow	6
2.2 Measurement Methods of Stream Discharge	7
2.3 Applicability of Remote Sensing in Stream Discharge Estimation	8
2.4 Estimation of Water Level and Discharge Using Satellite Altimetry	9
2.4.1 Satellite Altimetry: Introduction and Working Principle	11
2.4.2 Satellite Altimetry Products	13
2.5 Multispectral Satellite Data for Monitoring River Discharge	14
2.5.1 NIR Band Reflectance as Proxy of Discharge	16
2.5.2 Satellite Optical Data Sets	17
2.6 Multi-Mission Satellite Approach for River Discharge Estimation	18
2.7 Application of Artificial Intelligence in Hydrology	20
2.7.1 Long Short-Term Memory	22
2.8 Relevant studies in Mekong River Basin	25
<b>CHAPTER 3 STUDY AREA AND DATA</b>	<b>26</b>
3.1 Study Area	26
3.1.1 Climate	27
3.1.2 Hydrology	28
3.1.3 Land use and Land cover	30
3.2 Data	31
3.2.1 In-situ River Discharge	31
3.2.2 Satellite Altimetry Data for Water Level	32
3.2.3 Satellite Optical Data Sets	35
3.2.4 Basin Characteristics	36

<b>CHAPTER 4 METHODOLOGY</b>	<b>37</b>
4.1 Estimation of water level at different stations in Mekong River	37
4.1.1 Time Series Water Level from Satellite Altimetry	38
4.1.2 Densification of Altimetry derived Time Series Water Level at In-situ Stations	39
4.2 Daily discharge estimation by merging satellite optical and altimetry data	40
4.2.1 C/M from Satellite Optical Data Sets	41
4.2.2 Merging Multiple Satellite Datasets	42
4.2.3 Evaluation of the performance of Long Short-Term Memory Model	44
4.3 Development of a regional model for estimation of the river discharge	45
<b>CHAPTER 5 EXPECTED OUTPUTS</b>	<b>47</b>
<b>CHAPTER 6 PROPOSED TIME SCHEDULE</b>	<b>48</b>
<b>CHAPTER 7 PROPOSED BUDGET</b>	<b>49</b>
<b>REFERENCES</b>	<b>50</b>

## LIST OF TABLES

Table 2-1 Summary of Satellite altimetry missions	13
Table 2-2 Previous Studies using multi-mission approach for discharge estimation	19
Table 3-1 Country wise area in the Mekong River Basin	27
Table 3-2 Monthly Average Precipitations in the Mekong River Basin	28
Table 3-3 List of in Situ Gauge Stations in the Mekong Mainstream used this Study	32
Table 3-4 Major Features of the Radar Altimetry Missions used in this Study	34
Table 3-5 Major Features of the Optical Satellite Sensors used in this Study	36
Table 4-1 Basin attributes and parameters used for regionalization	46
Table 7-1 Proposed Budget for the Study	49

## LIST OF FIGURES

Figure 1-1 Global Distribution of Hydrologic Gauges	2
Figure 2-1 The Principle of Radar Altimetry Measurement	12
Figure 2-2 Spatial trend patterns in sea level over January 1993-2014 based on multi-mission satellite altimetry	12
Figure 2-3 Illustration of a Long-Short Term Memory unit	23
Figure 3-1 Map of Study Area	26
Figure 3-2 The Climatic zones of the Lancang Mekong Basin	28
Figure 3-3 Mean Annual Runoff in the Mekong River Basin	29
Figure 3-4 Maximum, minimum and mean annual flows at sites along the Lancang Mekong River	30
Figure 3-5 Land Use and Land Cover Map of Mekong River Basin	31
Figure 3-6 Virtual Stations Track along the Lancang Mekong River	33
Figure 4-1 Overall Methodological Framework for the study	37
Figure 4-2 Methodological Approach to Estimate Water Level using Satellite Altimetry	38
Figure 4-3 Methodological Framework for Discharge Estimation Merging Optical Sensor Data and Altimetry Data	41
Figure 4-4 A representation of wet and dry pixel reflectivity	42
Figure 4-5 Methodological Framework for Development of Regional Model for Discharge Estimation	45

## LIST OF ABBREVIATIONS

AI	Artificial Intelligence
AMR	Advanced Microwave Radiometer
AMSR-E	Advanced Microwave Scanning Radiometer for the Earth Observing System
ANN	Artificial Neural Network
CNES	Centre National d'Etudes Spatiales
CTOH	Center for Topographic Studies of the Ocean and Hydrosphere
DEM	Digital Elevation Model
DORIS	Doppler Orbitography and Radio-positioning Integrated by Satellite
ENVISAT	Environmental Satellite
EOS	Earth Observing System
ERS	European Remote Sensing satellite
ESA	European Space Agency
EUMETSAT	Exploitation of Meteorological Satellites
GDR	Geophysical Data Record
GEE	Google Earth Engine
GEOS-3	Geodynamics Experimental Ocean Satellite-3
GFO-RA	GEOSat Follow-On Radar Altimeter
GHz	Gigahertz
GNSS	Global Navigation Satellite System
GPS	Global Positioning System
GRDC	Global Runoff Data Centre
HY-2A	Hai Yang 2A
JPL	Jet Propulsion Laboratory
km	Kilometer
Ku band	Kurtz-under band
LRA	Laser Retroreflector Array
LRM	Low Resolution Mode
LSTM	Long Short-Term Memory
MLP-ANN	Multilayer perceptron Artificial Neural Network
mm	millimeter
MODIS	Moderate Resolution Imaging Spectroradiometer

MRC	Mekong River Commission
MWR	Microwave Radiometer
NASA	National Aeronautics and Space Administration
NIR	Near Infrared
NOAA	National Oceanic and Atmospheric Administration
NSE	Nash Sutcliffe efficiency
OSTM	Ocean Surface Topography Mission
PBIAS	percent bias
PLRM	Pseudo Low Resolution Mode
POD	Probability of Detection
$R^2$	coefficient of determination
RMSE	root mean square error
RNN	Recurrent Neural Network
RS	Remote Sensing
SAR	Synthetic Aperture Radar
SARAL	Satellite with ARGOS and ALtiKa
SDR	Stage Discharge Rating
SRAL	SAR Radar Altimeter
SWOT	Surface Water and Ocean Topography
TOPEX	The Ocean Topography Experiment
US	United States
VS	Virtual Station

# CHAPTER 1

## INTRODUCTION

### 1.1 Background of the Study

Water is nature's most valuable resource, and due to rising demand, fresh water supply is in risk of becoming non-renewable (Kim et al., 2008). Water covers over 71 percent of the Earth's surface. However, only 3% of this is fresh water, with the remaining 2.5% trapped in ice and glaciers. As a result, individuals must rely on 0.5% fresh water for all of their needs (Kashid & Pardeshi, 2014). Inland surface water bodies, such as lakes, reservoirs, creeks, streams, and rivers, are essential to our daily lives. Inland surface water sources provided the majority of the water needed for thermoelectric generation, public supply, agriculture, mining, and industrial purposes (Kenny et al., 2009).

The geographical and temporal patterns of water resource distribution are essential knowledge for water resource management and assessments of water vulnerability. River discharge is an important variable in hydrological studies and applications such as global change monitoring, flood risk assessments, water supply management, dam design, irrigation projects and many more (Van Dijk et al., 2016). River discharge monitoring is also important for establishing a better knowledge of changes in the water cycle and hydrological processes at river-basin scales and globally because of natural disasters and anthropogenic activities (Robert Brakenridge et al., 2012). The level of water bodies is a major concern when it comes to managing and monitoring inland water resources.

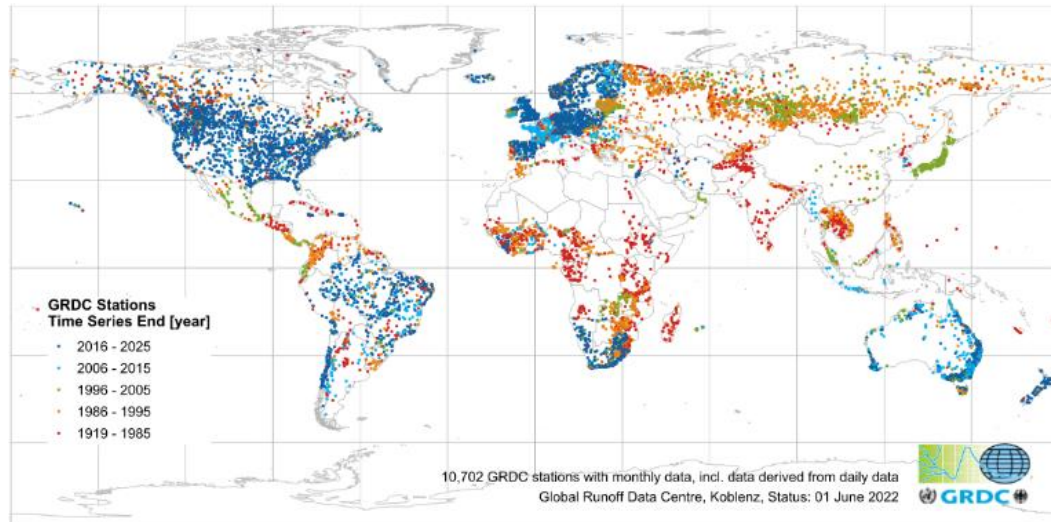
Mostly, estimation of river discharge has relied on network of gauging stations measuring water levels which capture data on water level at precise time intervals (Shi et al., 2020). In-situ networks of gauges that record water level at fixed points in rivers and lakes limits number of measurements of inland water bodies. The spatial distribution of gauge stations, on the other hand, is significantly uneven. In-situ gauge network implementation varies by location accessibility, and data availability is determined by national policies. It is also difficult and expensive to set up and maintain these networks in remote areas. Furthermore, the precision of readings is largely reliant on the processing method used and the current state of water bodies. During flood seasons and other extreme events, gauge stations are particularly vulnerable



(Biancamaria et al., 2010). Figure 1-1 depicts the global distribution of hydrologic gauges and their insufficient monitoring capability.

**Figure 1-1**

*Global Distribution of Hydrologic Gauges (GRDC Data Portal)*



Due to a lack of reliable measurements and insufficient in-situ gauge stations, an accessible and repeatable approach is a must for monitoring river discharge variations. Estimating river stage and discharge based on satellite-measured water level and inundation area is a reasonably easy and alternative method to overcome this issue (Huang et al., 2018). Broadly, use of remote sensing in discharge estimation are grouped into three categories: first category also called rating curve method uses stage-discharge relationship developed from remotely sensed water level or inundated areas with simultaneously collected in-situ data for discharge estimation, second category uses river water level or width from remote sensing data as input parameter or reference for calibration in hydrological or hydraulic models and third category also called remote sensing driven method uses remote sensing data as major input for estimation of river discharge (Shi et al., 2020).

Various studies have been carried out demonstrating applicability of satellite altimetry water level to estimate river discharge (Birkinshaw et al., 2010; Bogning et al., 2018; Calmant & Seyler, 2006; Jiang et al., 2017). However, the temporal resolution of water level and discharge is limited to 10 days (Topex/Poseidon, Jason 1/2/3) or 35 days (EnviSat, SARAL/ALTIKA) due to repeat period of satellite orbit (Tarpanelli, Barbeta,

et al., 2013). Moreover, use of optical sensors and passive microwave sensors in discharge estimation cannot be discarded since they have less revisit time almost daily and large coverage area. The reflectance ratio of land and water body (C/M) from Near Infrared (NIR) band of Moderate Resolution Imaging Spectroradiometer (MODIS), Landsat, Advanced Microwave Scanning Radiometer for the Earth Observing System (AMSR-E) and Global Flood Detection System (GFDS) has been successfully used as proxy for river discharge estimation (Brakenridge et al., 2005; Hou et al., 2018; Tarpanelli et al., 2019). Cloudy sky hinders the usability of optical sensors data which may result in data outages in measurements and the possible way to overcome is to use multi-mission satellite products to increase sample size (Tarpanelli et al., 2019).

Thus, optical sensor data can be merged with altimetry data to catch information affected by cloudy sky for optical sensors and to improve temporal sampling. Artificial Neuron Networks (ANNs) are used largely in remote sensing applications since they offer an easy but effective possibility of merging input data from different sources into the same retrieval algorithm.

## **1.2 Statement of the Problem**

Water supply planning and management, reservoir management and control, hydropower generation, flood prediction and control, understanding the global water cycle, and other hydrological applications all require accurate measurements of river discharge. To get an accurate measurement of discharge, most rivers require a series of flow velocity measurements in each sector of the cross section. Also, river discharge is frequently obtained from river stage measurements using the stage-discharge rating (SDR) curve to save expense, effort, and time. At several points along the river, in-situ gauge station would offer continuous and dependable river stage measurements (Liu et al., 2016).

However, erosion and sediment deposition processes in river channels and riverbanks constantly alter the geometry of channels, the stage-discharge relationship changes over time. As a result, a periodic comparison of the SDR curves to direct observations is required and hence river gauging stations are expensive, labor-intensive, and time-consuming to maintain (Pan, 2013). On other hand, the number of gauging stations has dropped on a global basis, which is especially problematic in the face of hydrological

regimes that have altered dramatically in recent years or will do so in the future due to climate change (Arnell & Gosling, 2013; Fekete & Vörösmarty, 2007.). Mekong is one of the such basin whose hydrology is altered due to impact of climate change and hydropower developments (Hoang et al., 2016).

Due to the length and remoteness of the Mekong River, installing and maintaining adequate gauge stations to monitor the whole river would be difficult. Other concerns in such transboundary river basin related to economic/political restrictions/data delay, for example, would result in data inaccessibility in certain locations and hence the practicality of obtaining timely and continuous observations at many points along the river continues to be a problem (Liu et al., 2016). Thus, spaceborne sensors can be utilized to address this situation because of the expanding number of earth observation satellites and their improved temporal and geographical resolution. Moreover, a regional model of Lancang Mekong River if developed utilizing the available in-situ data in different river reach and data obtained from satellite sensors will help to estimate discharge in ungauged reaches of the river.

### **1.3 Research Questions**

1. What will be the performance of Remote Sensing in river discharge estimation?
2. What is the spatial and temporal variation of discharge in ungauged reach of Lancang Mekong River?

### **1.4 Objectives of the Study**

The main objective of this research is to utilize multisource remote sensing datasets for river discharge estimation in the Lancang Mekong River Basin (LMRB).

To achieve this main objective, following specific objectives are set:

- i. To produce time series water level coping with the limitations of temporal and spatial resolution of satellite altimetry.
- ii. To use machine learning approach for daily discharge estimation by merging satellite optical sensor data and altimetry data.
- iii. To estimate the river discharge at ungauged locations and analyze its spatial and temporal variation in LMRB.

### **1.5 Scope and limitations of the Study**

- i. This study uses eight in-situ station data for developing a regional model for estimation of river discharge using remote sensing.
- ii. The artificial neural network Long Short-Term Memory (LSTM) will be used in the study.
- iii. Daily water level obtained from satellite altimetry products Envisat, Jason-1/2, Sentinel 3A and reflectance ratio of dry and wet pixel obtained from MODIS will be used as input to LSTM model.
- iv. The results of the study will rely on quality and quantity of secondary data.

## CHAPTER 2

### LITERATURE REVIEW

#### **2.1 Importance of Monitoring River Flow**

Monitoring and quantifying river flow is crucial for future forecasting as well as for the sustainable management of this valuable resource (E. Zakharova et al., 2020). Demand for more accurate, high frequency, and accessible water data is increasing because of growing populations and rival water priorities, including the preservation and restoration of aquatic ecosystems.(Hirsch & Costa, 2004; Arnell & Gosling, 2013). Numerous significant applications across a variety of scales necessitate an understanding of river discharge, including global water balances, engineering design, flood predictions, reservoir operations, navigation, water supply, recreation, and environmental management (Gravelle, 2015). For freshwater ecosystems, river flow regimes, such as long-term average flows, seasonality, low flows, high flows, and other forms of flow variability, are crucial (Arnell & Gosling, 2013).

Around the final quarter of the 19th century, technology developed hydroelectricity, and as a result, regular measurements of river flow started to spread globally to advantageous locations to gather data that would help with river discharge forecasting, ensuring continuous power production and water volumes in line with demand (Depetris, 2021). However, the present environmental/ climate catastrophe has introduced new difficulties to the initial uncomplicated objectives. In addition to altering precipitation patterns and the frequency of extreme weather events, climate change also introduces non-stationary characteristics to river flow series (Arnell & Gosling, 2013). Therefore, building solid hydrological data bases is even more crucial so that river management for flood control, water shortage, and water quality maintenance may be based on careful observations of the frequency and intensity of river flows (Derecki & Quinn, 1987).

It is important emphasizing here that, Oceania and Africa, for example, account for more than half of the rivers for which Milliman & Farnsworth, (2011) in their well-known synthesis, could find no hydrological data. Maintaining global river discharge databases is a challenging task and despite major improvements since river flow measurement began, the extensive gauging network is still far from perfect (Milliman & Farnsworth, 2011). For instance, the Global Runoff Data Centre (GRDC) only

includes a limited number of stations that are mostly determined by the participating nations. Additionally, hydrological data is often insufficient or partial, and changes that occur over time in gauging networks could be undetected (Depetris, 2021).

## **2.2 Measurement Methods of Stream Discharge**

Discharge measurements are carried out in natural watercourses to calculate the surface outflow of a basin, its periodic variability, and its outflow characteristics. Data on stream flow must be collected in a cohesive way, for a consistent period, with an assessment of the accuracy and uncertainty involved (Tazioli, 2011). The various methods of discharge estimation includes stream gauging using stage and rating curves, velocity point measurements and dilution gauging and use of current meters (Gravelle, 2015). Most hydrometric stations have a staff gauge, which continually records data during predetermined time intervals. The water level data may be transformed into data on river discharge using a stage-discharge relationship. While analytical formulae may be used to explain these relationships, it is preferable to collect experimental data and calibrate it using actual river discharge measurements (Perumal et al., 2007).

Obtaining mean flow velocity of the section, the traditional methods is carried out by submerging a current meter in several spots of a river cross-section (Tazioli, 2011). However, some problem arises in very high discharge, when water depth is insufficient for immersion of the equipment or flow velocity is lower than the minimum required, in case of turbulence. An alternative for these conditions is the artificial tracing method which is the use of radioactive substances or chemicals like sodium chloride (Florkowski et al., 1969).

To address the gap of on-site measurements, alternative methods of streamflow prediction and monitoring; modeling and satellite observations, have been rapidly developed. While satellite observation may give global views, hydrological modeling is a powerful tool for providing insights at regional or basin scales (E. Zakharova et al., 2020). Since river discharge cannot be monitored directly due to its nature, observations of other hydraulic variables, such as water level, flow velocity, water extent, and slope, both satellite and conventional monitoring methods is used to calculate river discharge (Bjerklie et al., 2005).

### **2.3 Applicability of Remote Sensing in Stream Discharge Estimation**

Remote sensing has developed as a reliable source of observations during the recent years, especially in regions of the world with scarce in situ networks (Bjerklie et al., 2018). There is currently no satellite-based technique that can measure river discharge directly. In order to estimate stream discharge, the use of remotely sensed hydraulic characteristics such water-surface width, gradient, and elevation has been investigated by many researchers (Bjerklie et al., 2005; Dingman & Bjerklie, 2005; Leon et al., 2006; Zakharova et al., 2020). Thus, satellite remote sensing is used to estimate a variety of hydrological status variables and fluxes. Though satellite remote sensing systems may make continuous and up-to-date measurements with broad area coverage depending on the orbital features of the platform, they depend on in-situ observations for algorithm development and validation (Tang et al., 2009).

Contrary to popular belief, remote sensing does not aim to completely replace gauges in discharge estimation (Gleason & Durand, 2020). Remote sensing for discharge estimation is therefore used for substitute of different purpose:

- At the mercy of politics and economics, gauges that exist now might not exist tomorrow.
- Remote Sensing signals are able to expand point gauge measurements in space and time due to high gauge calibration data.
- Water resources may be documented using Remote Sensing for Discharge in a variety of channel configurations and during times of flooding, which are challenges for gauges.
- Another area where Remote Sensing for Discharge may excel is with discontinued gauges, as these gauges can be calibrated and then utilized to parameterize models as they advance into the future.
- When creating a primary data source for usage in locations that are not well monitored, remote sensing might be utilized to prepare inaccurate data.

Bjerklie et al. (2003) assessed the possibilities of the various satellite data sources, described a variety of methods for using remote sensing to calculate river flow, and thought about the possibility of computing river discharge exclusively from remotely sensed data sources. In comparison to other models that merely contain width and slope

or width, slope and velocity, the authors contend that models based on these parameters are often more accurate, especially for big rivers.

Lin et al. (2019) created a cogent worldwide reanalysis of daily river discharge at approximately three million river reaches using a considerable amount of ground and remote sensing data (mostly for precipitation and evapotranspiration) along with the most recent advances in remote sensing hydrography. The power of remote sensing for global hydrologic modeling is illustrated by the level of temporal and spatial precision that has never before been attained. Lin et al. (2019) employed a calibration strategy that takes uncertainty into account, calibrating with gauges when available, remote sensing products when gauges are not, and reanalysis data when remote sensing and gauges are both accessible. This makes it feasible to produce discharge that wouldn't be possible without the use of remote sensing by making the best use possible of both in situ and remote sensing data.

Recent studies have shown that remote sensing has a strong spatial coverage and a longer monitoring period, both of which have driven an increase in interest in using remote sensing to predict discharge (Garkoti & Kundapura, 2021; Huang et al., 2018; Mengen et al., 2020; Sichangi et al., 2016).

#### **2.4 Estimation of Water Level and Discharge Using Satellite Altimetry**

Water levels in big rivers, lakes, and floodplains have been continuously monitored by satellite altimetry, and a time series spanning more than 25 years is now available (Papa et al., 2010). Several studies have demonstrated the capability of using satellite altimetry for estimating river discharge in medium to large rivers (with a width of few kilometers), including the Po River, Italy (Tarpanelli, Barbeta, et al., 2013), Niger River (Tourian et al., 2017), Ob River (Kouraev et al., 2004) and several location is Amazon river (E. A. Zakharova et al., 2006) with the use of rating curve developed by correlating altimetry river water level with in-situ measurements of river discharge or development of models.

Thus, the monitoring of river water levels has benefited from recent advancements in radar altimetry technology, and the increasing accuracy of the sensors supports their use as a validation tool for a variety of applications, from basic routing strategies to complex hydraulic models. Though the altimetry mission's spatial-temporal sampling



is a limitation (Tarpanelli et al., 2019). When the satellite ground track repeats (10-day TOPEX/Poseidon and Jason; 35-day ERS-2 and ENVISAT), this may be viewed as a space-borne virtual gauge that measures temporally distinct river channel stages. The upcoming Surface Water and Ocean Topography (SWOT) satellite mission will enhance the temporal and geographical coverage in the future (Birkinshaw et al., 2014).

Chen et al. (1998) demonstrated how models may be integrated with remote sensing to produce discharge using data from the Topex/Poseidon satellite to observe sea level changes and comprehend anomalies in sea surface heights. According to their argument, monitoring ocean anomalies can help us comprehend the necessary adjustments to the global hydrologic cycle that led to such anomalies if the ocean is the ultimate repository for all terrestrial water.

Birkinshaw et al. (2010) highlighted the possibility of employing remote sensing, such as SAR, to give information on the channel cross sections by combining altimetry data with in-situ observed channel cross sections to predict discharge at an ungauged location. The approach makes use of the cross-sectional regions upstream and downstream; altimetry provides the height variation and in situ or remote sensing data provides the river geomorphology. Remote sensing data in particular may be utilized to provide a time series of river width, which when combined with altimetry results in the cross-sectional area at the sub-satellite sites that changes over time.

In the research by Bogning et al., (2018), the performance of the five altimetry missions was evaluated by comparing the results to records from gauge station measurements. A long-term and vastly better water-level time series was produced by combining the data from all of the radar altimetry missions. An improvement in water level peak to peak characterization and, consequently, a more precise annual discharge throughout the shared observation period between the altimetry-based and the in situ mean annual discharge are both produced by the increased data sampling in the river basin.

This technique has however several limitations which includes dependence on quality of altimetry data over continental water bodies, unavailability of in-situ observations to develop rating curves, assumption of static rating curve while extending time series of discharge and temporal sampling rate (Papa et al., 2010).

### 2.4.1 Satellite Altimetry: Introduction and Working Principle

At the end of the 1960s, satellite radar altimetry first appeared. Based on active microwave observations (or radar) methods, radar altimetry measures distance. The electromagnetic (EM) pulse is transmitted in the nadir direction by the radar sensor, which then accurately calculates the signal's two-way travel time ( $\Delta t$ ). In order to record the radar echo or waveform, pulse compression and de-ramping methods are used. The waveform's amplitude and shape, which are connected to the backscattering coefficient, reveal details about the surface's makeup. When the received power reached the center of the leading edge at mid-height, the distance between the satellite and the surface, or altimeter range ( $R$ ), corresponded to that epoch. It is estimated as

$$R = \frac{c\Delta t}{2} \quad \text{Equation 2-1}$$

where  $c$  is the velocity of light in vacuum.

The range must be adjusted for atmospheric propagation delays, instrument corrections, and surface geophysical adjustments in order to calculate the surface topography accurately (Frappart et al., 2017). Using an ellipsoid to represent the sea-surface height (SSH) over the ocean as shown in Figure 2-1 and the height of the reflecting surface ( $h$ ) is then determined as;

$$h = H - R - \Delta R_{ion} - \Delta R_{dry} - \Delta R_{wet}(-\Delta R_{ssb}) \quad \text{Equation 2-2}$$

where  $H$  is the height of the center of mass of the satellite above the ellipsoid estimated using precise orbit determination techniques

$R$  is the nadir altimeter range from the center of mass of the satellite to the surface considering instrumental corrections

$\Delta R_i$  are the corrections applied to the range and applied over all types of surfaces

$\Delta R_{ion}$  is the atmospheric correction which is the atmospheric refraction range delay caused by the ionosphere's dielectric characteristics and free electron content

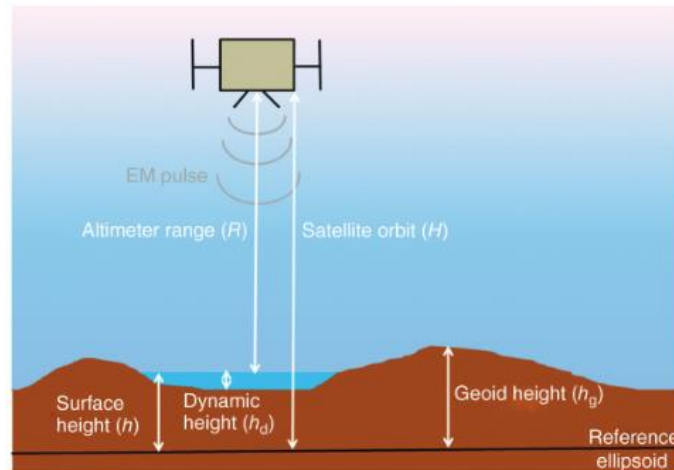
$\Delta R_{dry}$  is the atmospheric refraction range delay caused by the troposphere's dry gas component

$\Delta R_{wet}$  is the atmospheric refraction range delay caused by the tropospheric water content in clouds and water vapor

$\Delta R_{ssb}$  is the range correction over oceans and great lakes which is the interaction of the altimeter's electromagnetic pulse with the scatterers within the footprint (e.g., wave and surface roughness effects)

**Figure 2-1**

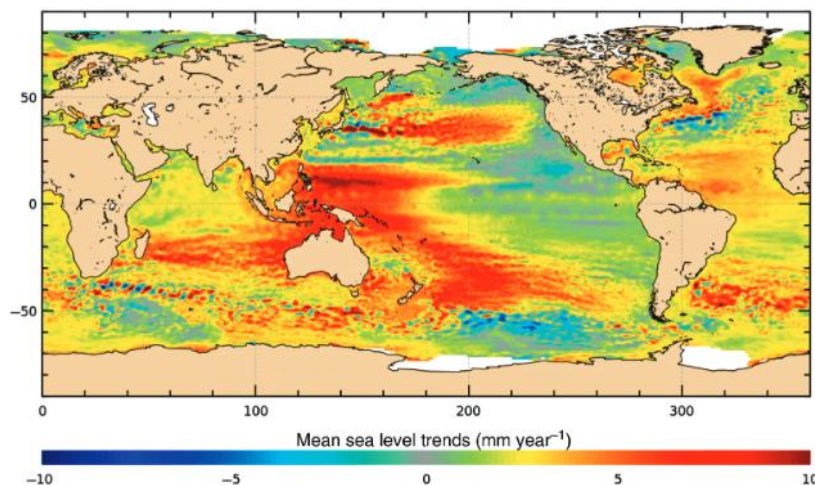
*The Principle of Radar Altimetry Measurement (Frappart et al., 2017)*



Originally, altimeter products have been used to monitor the surface elevation of oceans and study shows the rise in sea level is not constant. The pace of sea level rise in some areas (such as the western Pacific) is up to three times higher than the average rate worldwide which is shown in Figure 2-2. Later these altimetry satellite missions are being used for observation of large rivers and lakes for long-term observations of water level variations (Frappart et al., 2012).

**Figure 2-2**

*Spatial trend patterns in sea level over January 1993-2014 based on multi-mission satellite altimetry (<https://climate.esa.int/en/projects/sea-level/> )*



Satellite altimetry can help with hydrological research since it keeps track of surface water heights (Calmant & Seyler, 2006). Using specialized software like the Multi-mission Altimetry Processing Software, a more accurate selection of valid data may be made in order to increase the accuracy of the water stages generated from altimetry. The accuracy and bias of water stages estimated from radar altimetry were evaluated in several studies and found to have good accuracy compared with in-situ observations (Biancamaria et al., 2017).

#### 2.4.2 Satellite Altimetry Products

The time series of measurements of inland water levels that began with the launch of ERS-1 in 1991 and TOPEX/Poseidon in 1992 is continuously being extended by the availability of satellite altimetry from ERS-2 and ENVISAT as well as from Jason-1 and Jason-2 (Birkinshaw et al., 2010).

GEOS-3, SeaSat, Geosat, TOPEX/Poseidon, Geosat Follow-on, and Jason-1/2/3 from the National Aeronautics and Space Administration are among the previous and present satellite altimetry missions listed (NASA). These satellites include ERS-1/2, ENVISAT, CryoSat-2, and Sentinel-3 from the European Space Agency (ESA). Other missions, like the Chinese-planned HY-2A or the combined French-Indian SARAL/AltiKa project, are also in operation. The summary of satellite altimetry missions is shown in Table 2-1.

**Table 2-1**

*Summary of Satellite altimetry missions (Jiang et al., 2017)*

Satellite	Agency	Period	Altitude (km)	Altimeter	Frequency Used	Repetitivity (Day)	Equatorial Inter-Track Distance (km)
Skylab	NASA	May 1973–February 1974	435	S193	Ku-band		
GEOS3	NASA	April 1975–July 1979	845	ALT	Ku and C-band		
SeaSat	NASA	July–October 1978	800	ALT	Ku-band	17	
Geosat	US Navy	October 1985–January 1990	800		Ku-band	17	

Satellite	Agency	Period	Altitude (km)	Altimeter	Frequency Used	Repetitivity (Day)	Equatorial Inter-Track Distance (km)
ERS-1	ESA	July1991– March2000	785	RA	Ku-band	35	80
Topex/ Poseidon	NASA/ CNES	September1992 – October2005	1336	Poseidon	Ku and C-band	10	315
ERS-2	ESA	April1995- July2011	785	RA	Ku-band	35	80
GFO	US Navy/ NOAA	February1998– October2008	800	GFO-RA	Ku-band	17	165
Jason-1	CNES/ NASA	December2001– June2013	1336	Poseidon- 2	Ku and C-band	10	315
Envisat	ESA	March2002– April2012	800	RA-2	Ku and S-band	35	80
OSTM/ Jason-2	CNES/ NASA/ Eumetsat/ NOAA	Jun2008– present	1336	Poseidon- 3	Ku and C-band	10	315
CryoSat- 2	ESA	April2010– present	720	SIRAL	Ku-band	369	7.5
HY-2	China	August2011– present	971		Ku and C-band	14168	
Saral	ISRO/ CNES	February2013– present	800	AltiKa	Ka-band	35	80
Jason-3	CNES/ NASA/ Eumetsat/ NOAA	January2016– present	1336	Poseidon- 3B	Ku and C-band	10	315
Sentinel- 3A	ESA	February2016– present	814	SRAL	Ku and C-band	27	104

## 2.5 Multispectral Satellite Data for Monitoring River Discharge

Recent developments in satellite sensors stimulated its use for river flow estimation due to their frequent revisit time and large spatial coverage, taking into account the daily river discharge measurement (Filippucci et al., 2022). Several studies have shown the possibility of discharge estimation from the space with their feasibility to monitor difficult river sites in medium-sized to large catchments from various sensors, including

MODIS, MERIS, Landsat and OLCI datasets (Brakenridge & Anderson, 2006; Shi et al., 2020; Tarpanelli, Brocca, et al., 2013; Tarpanelli et al., 2020). Since discharge cannot be measured directly, hydraulic variables like river channel widths and the extent of surface water are measured using remote sensing data. This information can be gathered by synthetic aperture radar (SAR), visible spectrum digital imagery and they have been used to monitor the extent of a floodplain's inundation, cross section geometry and variation of water level with river extent (L. Smith & Pavelsky, 2008; Sun et al., 2010).

There are two main approaches for monitoring river discharge via multispectral images. One method is to develop regression relationship between in-situ measured discharge and inundated channel reflectivity (including inundated and potentially inundated area of the river channel) and other is to develop regression relationship between river width and in-situ discharge. Both of these methods have been used successfully in various river for discharge estimation (Bjerklie et al., 2003; Li et al., 2019; L. C. Smith & Pavelsky, 2008; Tarpanelli, Brocca, et al., 2013)

Brakenridge & Anderson (2006) proved the practical hydrological uses of the Moderate resolution Imaging Spectroradiometer (MODIS) sensor, including not only flood detection and characterization but also discharge estimates. They only provided one early example where MODIS approximated the discharge using a very short time period (about 30 data).

Sichangi et al. (2018) computed temporal river width data from the MODIS images to derived river discharge. Only remote sensing data with NSE values larger than 0.5 at the analyzed sites were used to estimate discharge. The calculated velocity's values, which range from 0.63 to 1.2 m/s and 0.81 to 1.35 m/s, were found to be within the bounds of the expected velocity 0.96 m/s. The methodology for calculating discharge is a viable strategy for usage on rivers all across the world because it exclusively relies on global satellite databases.

Sahoo et al. (2020) presented an integrated MODIS-Landsat fusion methodology and tested the method in eastern India's Brahmani River Basin to estimate high-frequency discharge. To increase the temporal resolution of the single datasets, a copula-based model was suggested, and the improved results were then shown. This study on the use

of many satellites for different missions demonstrated their value in improving flow monitoring, particularly in highly forested areas.

### ***2.5.1 NIR Band Reflectance as Proxy of Discharge***

Optical remote sensing sensors are the essential tools that measure various spectral signatures, according to wavelengths, that each sensor monitors reflected or emitted energy. However, optical remote sensing images are impacted by clouds, haze, and cloud shadows, making it difficult to distinguish between them and other dark objects like water and shadows (Zhu & Woodcock, 2012). In near infrared (NIR) wavelengths, water absorbs more energy (has a low reflectance), whereas non-water reflects more energy (high reflectance) because of the strong water absorption in NIR (Ahn & Park, 2020). Any location that experiences flooding will have an increase in water surface, which will lower the area's NIR reflectance value as seen by the satellite. This different spectral characteristics of water bodies and other objects in near-infrared (NIR) images can be used to monitor variations in the river discharge (Shanlong et al., 2010).

The Calibration/Measurement (C/M) technique makes use of the relationship between surface water extent dynamics and river flow. This method is based on the principle that the ratio of reflectivity from non-inundated area and the inundated area is positively correlated with river discharge. First, Brakenridge et al. (2007) used AMSR-E data at 37 GHz to estimate river flows using the difference between the brightness temperature of a pixel over the river and a pixel over an unaffected pixel. Subsequently, MODIS sensor had been used successfully exploiting different behavior of land and water in NIR band for discharge estimation (Sahoo et al., 2020a; Van Dijk et al., 2016). In contrast, if light, atmospheric scattering, or vegetation characteristics change and recorded radiances change simultaneously, the ratio stays fairly constant. Utilizing MODIS optical data to detect surface water changes economically and effectively is the paired-measurement method (Brakenridge et al., 2005).

While many traditional sensors can readily capture surface water dynamics, the C/M technique has the benefit of requiring less data. The C/M technique may be broadly divided into two categories: one uses optical satellite data, such as the near-infrared (NIR) band of the Moderate Resolution Imaging Spectroradiometer (MODIS). The other uses microwave satellite data such as that from the Advanced Microwave Scanning Radiometer for the Earth Observing System (AMSR-E), to estimate discharge

and identify floods, even in rivers that are not gauged and are inaccessible. The AMSR-E method of performing C/M is a more complicated procedure that necessitates other auxiliary data, such a precipitation dataset, at the same time (Temini et al., 2011).

Tarpanelli, Brocca, et al. (2013) used this method and successfully predicted discharge for four sections of the Po River in northern Italy using M and C pixels from MODIS NIR images. This work has demonstrated that MODIS data may be used for ungauged river sites as well as medium-sized basins (<10,000 km<sup>2</sup>) with considerable temporal variability to provide reliable flow estimates.

Shi et al. (2020) applied linear regression between C/M with observed discharge series using Harmonized Landsat and Sentinel-2 (HLS) surface reflectance product on relatively small rivers with 30~100 m widths in Murray Darling Basin, Australia to estimate river discharge. The results showed high consistency with the observed discharge.

### 2.5.2 Satellite Optical Data Sets

The multispectral image data can be obtained for different satellite missions. These data availability depends upon the orbital period of satellite and their spatial and temporal resolution. Terra and Aqua satellites both have the MODIS instrument in operation. Every one to two days, it observes the whole surface of the Earth within a 2330-kilometer viewing swath. With three different spatial resolutions of 250 m, 500 m, and 1000 m, its detectors measure 36 spectral bands between 0.405 and 14.385 m (MODIS Web). Likewise the details of other satellite missions are provided below.

S.N.	Data	Agency	Equatorial cross-track separation (km)	Spatial Resolution	Temporal Resolution	Period	Source
1	MODIS AQUA	NASA	2330	250 m, 500 m, 1000 m	1 – 2 days	May 2002 - Present	<a href="https://lpdaac.usgs.gov/">https://lpdaac.usgs.gov/</a>
2	MODIS TERRA	NASA	2330			Dec 1999 - Present	
3	Landsat ETM +	NASA and USGS	185	30m	16 days	Apr 1999 – Sep 2021	
4	Sentinel 2	ESA	290	10 - 60 m	5 days	June 2015 - Present	<a href="https://sentinels.copernicus.eu/">https://sentinels.copernicus.eu/</a>
5	Meris	ESA	1150	300 m	3 days	2002 - 2012	<a href="https://www.esa.int/">https://www.esa.int/</a>



## **2.6 Multi-Mission Satellite Approach for River Discharge Estimation**

The estimations of discharge generated by combining the river stage level from satellite altimetry data with other space-based parameters, such as river width and river bed velocity from optical sensors and Synthetic Aperture Radar (SAR), ought to be superior to those based on a single parameter (Sichangi et al., 2016). Satellite altimetry has a relatively poor spatial sampling that corresponds to its ground track pattern ranging from 10 days for Jason series, 35 days for ERS, Envisat and Saral/AltiKa to 369 days for CryoSat-2 missions. Thus, multi-mission approach has been widely accepted and used in many studies to cope with the limitation of spatiotemporal resolution (Table 2-2) of satellite altimetry and optical images.

The approach involving use of altimetry and optical sensors for river discharge estimation has shown better performance in Niger and Po rivers with NSE of 0.98 and 0.83 (Tarpanelli et al., 2019).

**Table 2-2***Previous Studies using multi-mission approach for discharge estimation*

<b>Author</b>	<b>Study Area</b>	<b>Data Used</b>	<b>Method</b>	<b>Key Results</b>
Sichangi et al. (2016)	Eight of the world's major rivers	Envisat, Jason 2, MODIS and DEM	River stage is incorporated with the effective river width and compared with empirical equation proposed by (Bjerklie et al., 2003)	Improved prediction accuracy in most of the river.  NSE varied between 0.6 and 0.97 with $R^2 > 0.90$ .
Huang et al. (2018)	Upper Brahmaputra River, China	Jason 2/3, Saral AltiKa Landsat 5/7/8 and Sentinel 2 images	Modified Manning's equation and Rating Curve	The NSE vary between 0.65 to 0.97 and RMSE vary between 32.97 to 695 m <sup>3</sup> /s.
Bjerklie et al. (2018)	Yukon River, North America	Jason 2 Landsat	Manning's equation and Prandtl-Von Karman equation	The calibrated discharge estimate showed the accuracy of +/- 2%
Garkoti & Kundapura, (2021)	Krishna River, India	Jason 3, Sentinel 3A, Sentinel 3B, Sentinel 1 and Sentinel 2 images	Modified Manning's equation	The NSE vary between 0.53 to 0.62 and $R^2$ vary between 0.83 to 0.97.
Scherer et al. (2020)	Lower Mississippi River	Envisat, Jason-2/3, Sentinel-3A/3B, Landsat-4/5/7/8, Sentinel 2A/2B	Manning's equation	Estimate 18 years discharge time series using satellite altimetry and remote sensing data with NRMSE 7 – 35 %

## **2.7 Application of Artificial Intelligence in Hydrology**

John McCarthy first used the term "artificial intelligence" in 1956. The field of computer science known as artificial intelligence (AI) is concerned with the research and development of intelligent agents that can comprehend their surroundings and take actions that increase their chances of success. The definition of artificial intelligence (AI) is "the capacity to simultaneously hold two different ideas while retaining the capacity to function." However, AI must also have the capacity for inference, quick response, and learning from prior experience (Singh et al., 2013).

Machine learning is an application to AI. It is the practice of assisting a computer in learning without direct instruction by applying mathematical models of data. As a result, a computer system can keep picking up new skills and getting better on its own. Using a neural network, which is a collection of algorithms based after the human brain, is one method for teaching a computer to imitate human reasoning. Machine learning has been effectively used in remote sensing for source separation, classification, regression, clustering, and coding (Camps-Valls, 2009).

In order to predict different hydrological parameters, artificial neural networks (ANNs) are often and accurately employed; yet they are typically only created in one or two hidden layers. In order to successfully address complicated issues, deep learning networks have recently been enlarged with multi-layered design. A recent method of using ANNs is deep learning, which is a subfield of machine learning. It is used to represent complicated ideas by learning at various depths and levels. The unpredictable, complex, and nonlinear character of streamflow makes it viable to utilize AI-based modeling techniques. ANNs can mimic streamflow in particular using additional hydrological factors (Bengio, 2009; Ghumman et al., 2011).

Finding a suitable deep-learning network to use is challenging. However, this variety and adaptability could occasionally result in choosing the incorrect type of network from among the many options. Recurrent neural network (RNN) types of neural networks are an excellent substitute for continuous (time-series) data, such as streamflow, according to recent research (Elumalai et al., 2017). Long-term dependencies between the network's inputs and outputs could be discovered through Long Short-Term Memory (LSTM). Better model performance has been achieved using

this method, highlighting the LSTM's potential for application in hydrological modeling applications (Kratzert et al., 2018).

Several research have been done to address the application of machine learning in the field of hydrology. Some of the researches are discussed below:

Esmacilzadeh et al. (2017) used data-mining techniques such as ANNs, the M5 tree method, support vector regression, and hybrid Wavelet-ANN methods to estimate the daily flow to the Sattarkhan Dam in Iran. The wavelet artificial neural network (WANN) method outperformed other methods, according to the results, in estimating flow.

According to Kratzert et al. (2018), who used the publicly available CAMELS dataset to model daily streamflow in 291 catchments, the LSTMs as individual catchment models performed better primarily in snow-driven catchments and worse in arid basins because long-term dependencies are more significant for snow-driven processes (e.g., snow accumulation and snowmelt). Additionally, the LSTM model outperformed the benchmark conceptual model by a small margin.

Zhang et al. (2018) calculated water tables in agricultural areas using LSTM-RNN. They contrasted the simulation produced by LSTM-RNN with that produced by Multilayer Perceptron (MLP) and discovered that the former performed better than the latter. So, they suggested model can be used as a substitute for existing methods of estimating water table depth, particularly in locations where hydrogeological data are challenging to come by.

Chiang et al. (2018) combined ensemble approaches into artificial neural networks in order to lower the level of model uncertainty in hourly streamflow projections in the Chinese watersheds of Longquan Creek and Jinhua River. Results showed that as compared to a single neural network, the accuracy of streamflow predictions was enhanced by roughly 19–37% by ensemble neural networks.

According to Kao et al. (2020) the Shihmen Reservoir watershed in Taiwan experienced multi-step-ahead flood forecasting using the LSTM-based Encoder-Decoder (LSTM-ED) model,. Results indicated that the suggested model may boost the interpretability

of the model internals and raise the reliability of flood forecasting by converting and connecting the rainfall sequence with the runoff sequence.

Cheng et al. (2021) developed three machine learning models using ANN, Support Vector Regression (SVR), and LSTM to anticipate discharge variation in North China and adequate accuracy was attained. The results showed that MLP performed marginally better than LSTM-RNN and much better than SVR. Additionally, it was shown that ANNs were more effective than other machine learning techniques for modeling and forecasting karst spring outflow.

### ***2.7.1 Long Short-Term Memory (LSTM)***

A unique variety of RNN, known as the LSTM architecture, a type of model or framework for sequential data, was created to address the typical RNN's inability to learn long-term dependencies. It implements gates that control "memory cells" using a unique combination of hidden units, elementwise products, and sums between units. These cells are made to store data unaltered over extended periods of time (Hochreiter & Schmidhuber, 1997). The key advantage of LSTM is that it can learn long-term dependence, which is not achievable with straightforward RNNs.

Runoff was modelled for Fen River basin, China by Hu et al. (2018) using traditional ANN and LSTM models by and results showed LSTM performed better in terms of time series discharge simulation. The LSTM model is more cognitive than the ANN model, and the ANN model is more sensitive when compared to simulations of flooding events.

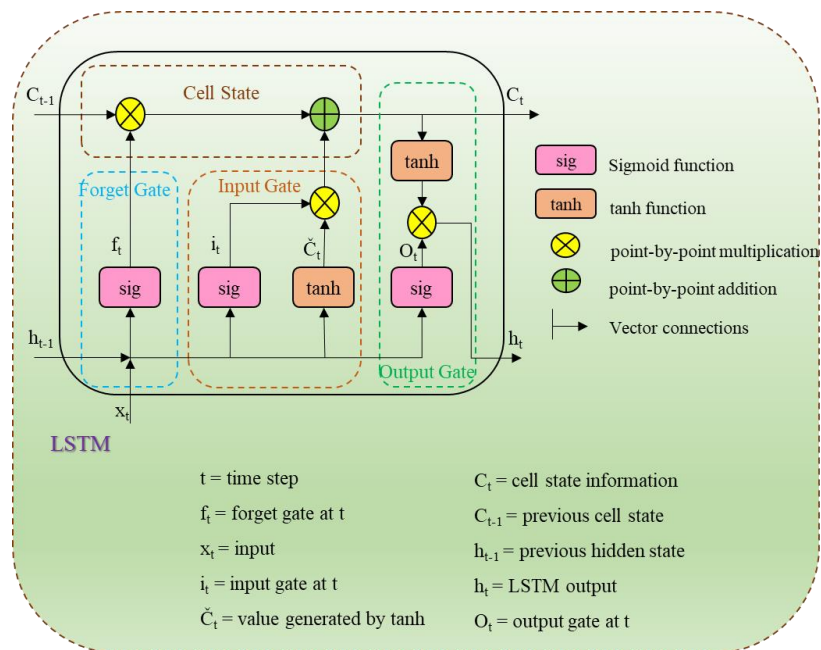
Nogueira Filho et al. (2022) studied the application of LSTM as a regional method against traditional neural network (FFNN) and conceptual models in a data scarce catchment. The LSTM model outperformed the Feedforward model in the specific catchment, demonstrating its ability to explain the hydrological dynamics of streamflow in semiarid areas. The performance of the neural networks trained with the regionalization data were better than the neural networks built for single catchments and the neural network approaches also exhibited the capacity to aggregate process understanding from diverse watersheds.

## LSTM Architecture

Figure 2-3 depicts the basic LSTM unit, which consists of a cell with an input gate, output gate, and forget gate. To handle the disappearing or ballooning gradient problem, LSTMs employ the idea of gating (Greff et al., 2017). Each of the three gates can be thought of as a typical artificial neuron, computing an activation (using an activation function) of a weighted sum of the current data  $x_t$ , a hidden state  $h_{t-1}$  from the previous time step, and any bias  $b$ . The cell is in charge of remembering values over arbitrary time intervals (Ordóñez & Roggen, 2016).

**Figure 2-3**

*Illustration of a Long-Short Term Memory unit*



**Forget gate** determines what information must be remembered and what can be forgotten. The sigmoid function receives data from the current input  $X_t$  and the hidden state  $h_{t-1}$ . The values that Sigmoid produces range from 0 to 1. It draws a conclusion on the necessity of the old output's portion (by giving the output closer to 1). The cell will eventually utilize this value of  $f_t$  for point-by-point multiplication.

$$f_t = \sigma(W_f \cdot [h_{t-1}, x_t] + b_f)$$

**Input gate** performs the following operations to update the cell status.

First, the second sigmoid function receives two arguments: the current state  $X_t$  and the previously hidden state  $h_{t-1}$ . Transformed values range from 0 (important) to 1. (not-important).

The tanh function will then get the identical data from the hidden state and current state. The tanh operator will build a vector ( $C_t$ ) containing every possible value between -1 and 1 in order to control the network. The output values produced by the activation functions are prepared for multiplication on a point-by-point basis.

$$i_t = \sigma(W_i \cdot [h_{t-1}, x_t] + b_i)$$

$$C_t = \tanh(W_c \cdot [h_{t-1}, x_t] + b_c)$$

**Output gate** determines the value of the next hidden state. Information about prior inputs is contained in this state.

First, the third sigmoid function receives the values of the current state and the prior hidden state. The tanh function is then applied to the new cell state that was created from the original cell state. These two results are multiplied one by one. The network determines which information the hidden state should carry based on the final value. For prediction, this concealed state is employed.

The new hidden state and the new cell state are then carried over to the following time step.

$$o_t = \sigma(W_o \cdot [h_{t-1}, x_t] + b_o)$$

$$h_t = o_t * \tanh(C_t)$$

At conclusion, the forget gate selects whatever pertinent information from the earlier processes is required to conclude. The output gates complete the next concealed state, while the input gate determines what pertinent information may be supplied from the current stage.

## 2.8 Relevant studies in Mekong River Basin

Several studies have been conducted in Lancang Mekong River Basin for the estimation of river discharge using remote sensing. Some of them are discussed.

Multi mission radar altimetry has been used to develop multiple rating curve and combined in an Ensemble Learning Regression method to estimate discharge (ELQ) at three locations: Stung Treng, Kratie, and Tan Chau in Lower Mekong River (Kim et al., 2019). Since the ELQ approach corrects for deterioration in the performance for Q estimation caused by the poor rating curve with virtual stations far from in-situ Q stations, various H derived from Jason-2 altimetry were employed in this study regardless of distances from in-situ Q stations. Compared to data obtained from a single rating curve, the ELQ estimated discharge revealed more accurate results.

Birkinshaw et al. (2014) estimated discharge for ten years at Nakhon Phanom and Vientiane on the Mekong River using (Bjerklie et al., 2005) equation. Landsat satellite imagery was utilized to offer a variety of channel widths over a stretch of river, while ERS-2, ENVISAT, and satellite altimetry data were used to produce a time series of river channel water levels and the channel slope. The performance evaluation gave Nash–Sutcliffe efficiency value of 0.90 for Nakhon Phanom and 0.86 for Vientiane to obtain river discharge.

A novel decile thresholding method was developed by Mungen et al. (2020) using the concept of at-many-stations hydraulic geometry (AMHG) in Mekong River. The peak flows are virtually always underestimated even though the decile thresholding method produces good results in the low-flow range. The decile thresholding discharge estimation outperformed the Gleason and Wang's optimized AMHG technique, with an RRMSE of 19.5 percent for the overall examined period and 16 percent for just the dry seasons.

However, the discharge estimated by above and other studies are site specific only and no studies have been carried out to develop regional model for whole river. This study is intended to develop a single regional model which can be used to predict discharge at ungauged sites of the river.



## CHAPTER 3

### STUDY AREA AND DATA

#### 3.1 Study Area

Large rivers including the Yangtze, Salween, Irrawaddy, Red River, and Mekong originate on the Tibetan Plateau. The Mekong drains an area of around 795,000 km<sup>2</sup> from its source and travels south for another 5000 km to the sea. It rises on the Tibetan Plateau and flows through the Yunnan Province of China, Myanmar, Laos, Thailand, Cambodia, and Vietnam. The country wise areas in the Mekong River Basin is shown in Table 3-1 . The Greater Mekong River can be divided into two basins: the Upper Basin, where the river is known as the Lancang and is located in Tibet and China; and the Lower Mekong Basin, which runs from Yunnan to the Sea (Figure 3-1).

**Figure 3-1**

*Map of Study Area*

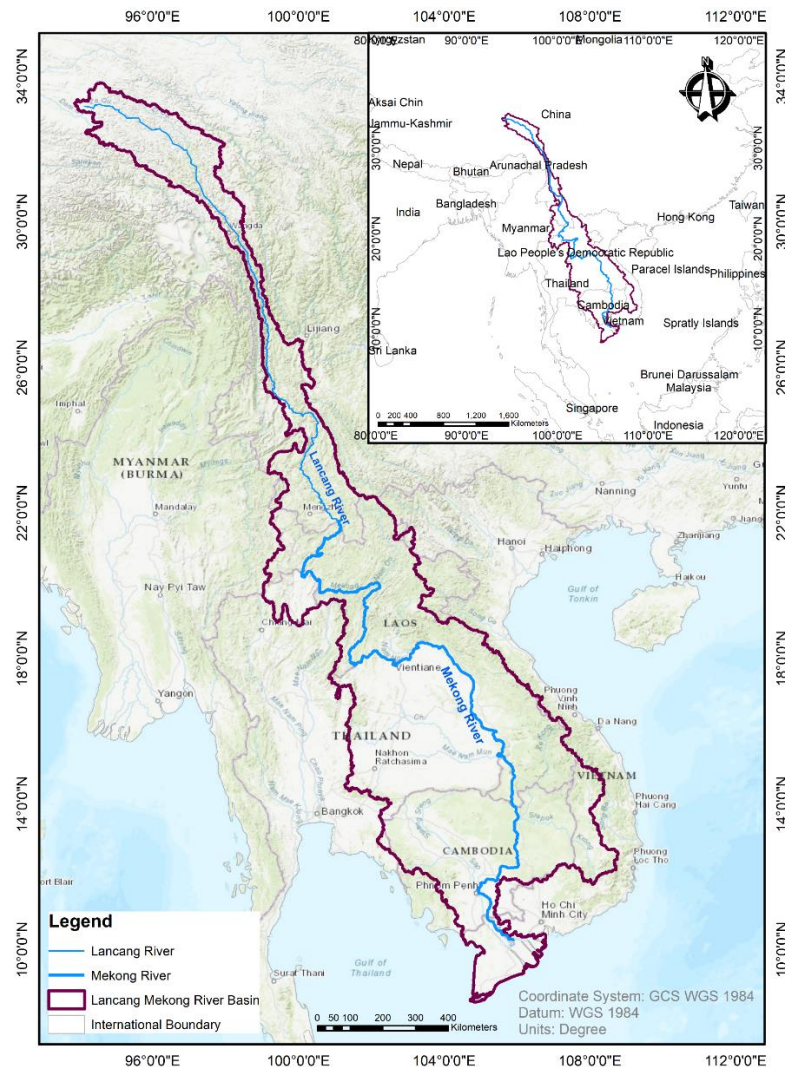


**Table 3-1***Country wise area in the Mekong River Basin*

<b>Basin</b>	<b>Area (km<sup>2</sup>)</b>	<b>Countries</b>	<b>Area of country in basin (km<sup>2</sup>)</b>	<b>% of the total area of the basin</b>	<b>% of the total area of the country</b>
Mekong	795,000	China	165,000	21	2
		Myanmar	24,000	3	4
		Lao PDR	202,000	25	85
		Thailand	184,000	23	36
		Cambodia	155,000	20	86
		Vietnam	65,000	8	20

The Upper Basin (China and Myanmar), which contributes around 15% of the flow, accounts for 24% of the entire catchment. There are no large tributaries, therefore all future water resource development will follow the main Mekong. On the other hand, the Lower Mekong Basin is also nourished by sizable tributaries, which account for around 85% of the annual flow.

### **3.1.1 Climate**

In the region upstream, the climate is cold, whereas in the region downstream, the climate is tropical. Yunnan province in southern China's Upper Basin also experiences monsoons, though there are significant topographic variations. Yunnan has a variety of climates, from subtropical and tropical monsoons in the south to temperate monsoons in the north. However, in Yunnan province, there is a significantly broader variance from year to year in the timing of the start of the southwest monsoon, which affects the pattern of rainfall in the Upper Basin of China. Although yearly levels drop to as little as 600 mm in the north, the seasonal pattern of rainfall is the same as for the Lower Basin. The variations in climatic zones of the Lancang Mekong Basin is shown in Figure 3-2.

The southwest monsoon, which typically lasts from May through late September or early October and coincides with the Lower Basin's flood season, dominates the region's climate. In most areas of the basin, there are frequent periods of intense rainfall lasting one or two days. The wettest months of the year are August, September, and in the delta even October due to tropical cyclones that affect most of the region later in the season. Less than 1,500 mm of rain fall each year averages throughout the floodplain of Cambodia and the Mekong Delta, while more than twice that amount falls in the

Central Highlands of the Lao People's Democratic Republic and inside the major valley at Pakse (MRC 2005). The precipitation between upper Mekong and Lower Mekong is quite different and presented in Table 3-2.

**Figure 3-2**

*The Climatic zones of the Lancang Mekong Basin (He et al., 2009)*

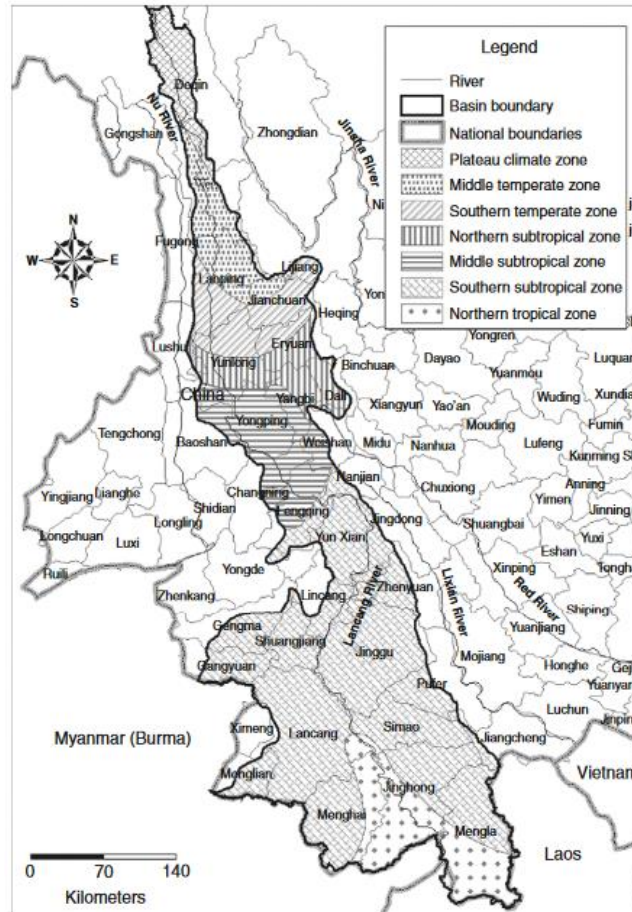


**Table 3-2**

*Monthly Average Precipitations in the Mekong River Basin (in mm) (He et al., 2009)*

Basin	Month	January	February	March	April	May	June	July	August	September	October	November	December	Annual
Upper Mekong	Rainfall	17	19	27	41	98	174	224	228	132	102	43	19	1125
	%	1.52	1.65	2.43	3.67	8.70	15.5	19.9	20.3	11.7	9.10	3.81	1.72	100
Lower Mekong	Rainfall	8	15	40	77	198	241	269	292	299	165	54	14	1672
	%	0.5	0.9	2.4	4.6	11.8	14.4	16.1	17.5	17.9	9.9	3.2	0.8	100

### 3.1.2 Hydrology

The Mekong River ranks eighth in the global basins with a mean annual flow into the South China Sea of around 14,500 m<sup>3</sup>/s. Although the flow from the Upper Basin makes up just 13% of the normal annual flow, it may make up to 30% of the flow during the

dry season (MRC 2010). A large network of tributaries makes up the Mekong River basin, creating several sub-basins. In the Lower Basin, significant tributary networks emerge. These systems may be split into two categories: those that contribute to the main rainy season flow and those that drain low relief areas with lesser rainfall. Tropical monsoonal regions are typically characterized by an abundance of water and a relatively consistent flow pattern. However, the flow continues to vary dramatically from year to year (MRC, 2018). The estimated mean annual flow of the basin is almost 460 km<sup>3</sup> and of the total annual flow, in an average year about 75 per cent occurs within just four months between July and October.

The mean annual runoff in the basin is shown in Figure 3-3. In the Lancang Mekong watershed, river discharge rises sharply from north to south, with significant regional variations which is shown in Figure 3-4.

**Figure 3-3**

*Mean Annual Runoff in the Mekong River Basin (MRC, 2010)*

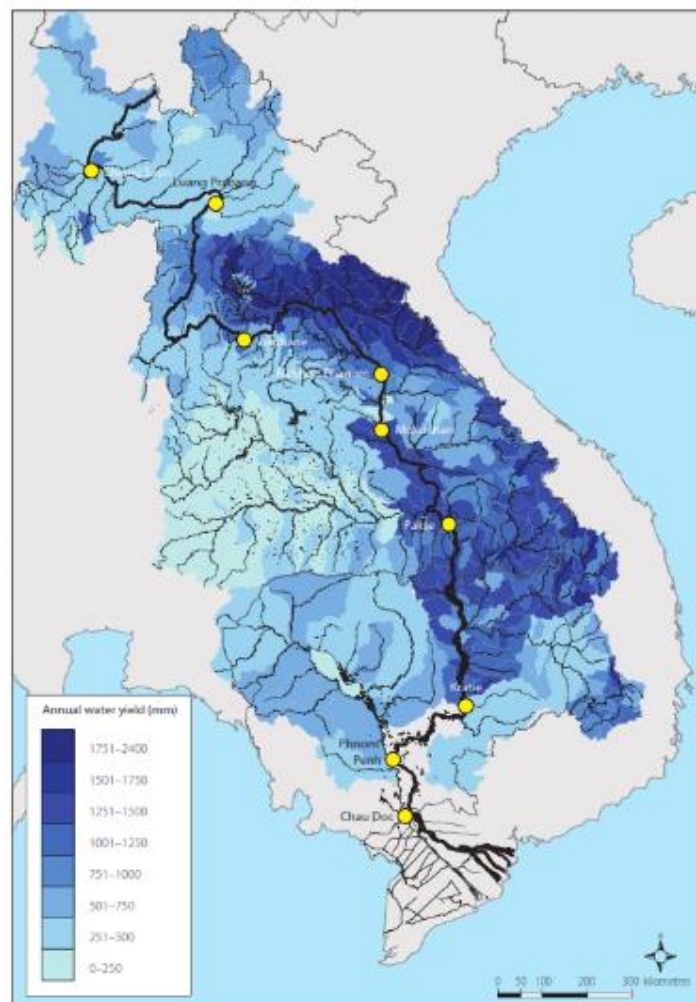
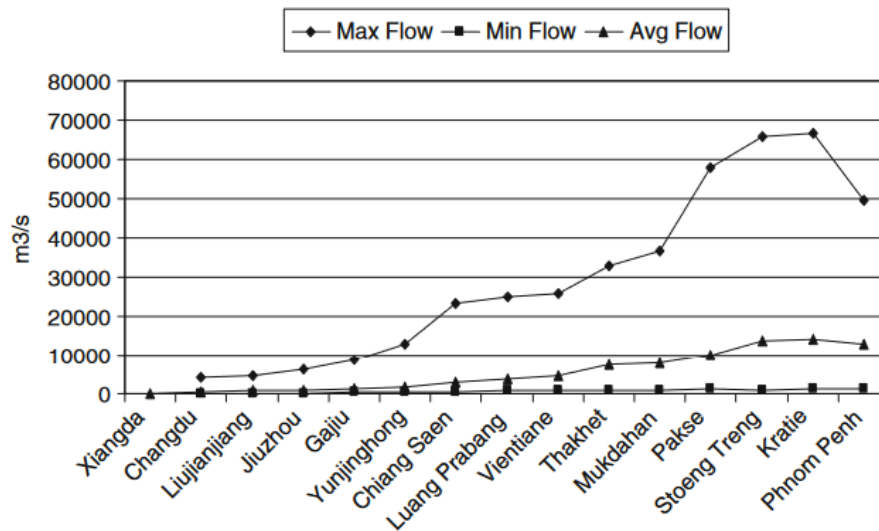


**Figure 3-4**

*Maximum, minimum and mean annual flows at sites along the Lancang Mekong River (He et al., 2009)*



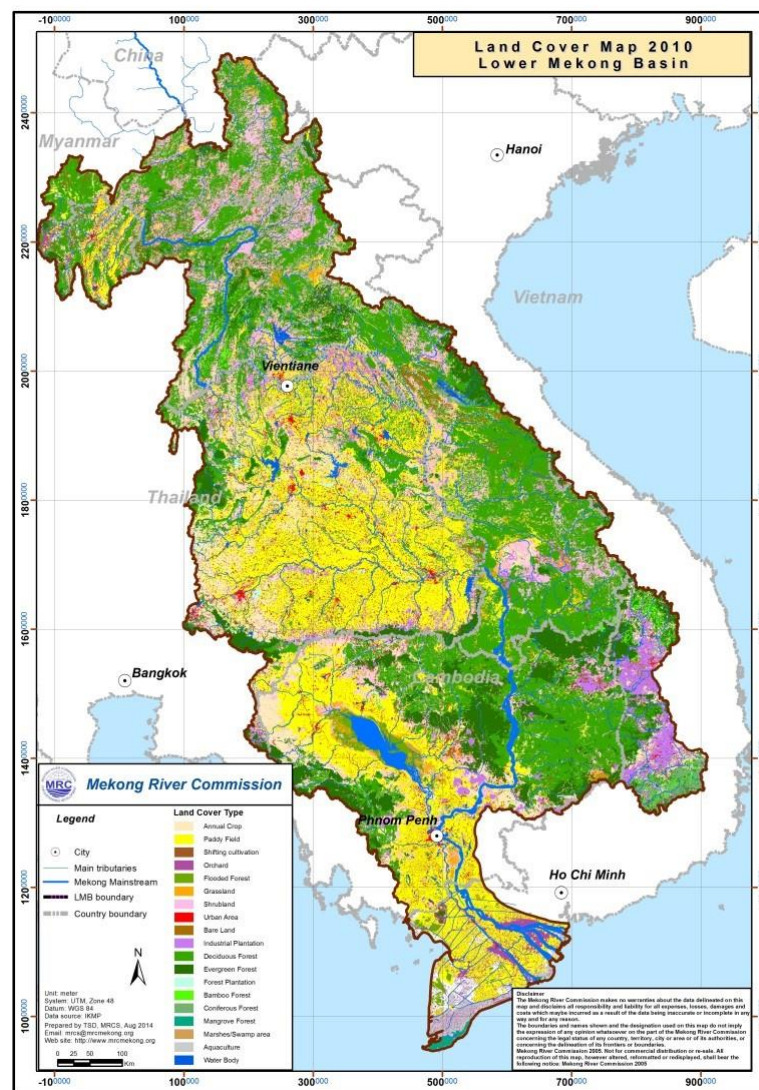
### **3.1.3 Land use and Land cover**

The river and its tributaries are constrained by narrow, steep gorges in the upper Mekong River Basin. In this region of the basin, there are few tributary river systems. The river alters as the floodplain widens, the valley expands, and the river widens and slows. Soil erosion is the main issue here. The primary determinants of the river's hydrology are the climate, geography, and land use of the lower Mekong Basin. The soils recover after upland shifting agriculture (slash and burn), but the vegetation takes much longer. Similar to other areas of the basin, shifting and permanent cultivation have gradually decreased the amount of forest cover over the past three decades. Over the past 50 years, Thailand's Lower Basin regions have had the greatest rate of forest cover loss among all the countries along the Lower Mekong. The land use and land cover map of the Mekong Basin is presented in Figure 3-5.

The most prevalent soil types are salty and sandy, making a large portion of the area unsuitable for growing wet rice. However, agriculture is intense despite the low fertility. The main crops are cassava, maize, and glutinous rice. The main hydrological risk in this area is drought.

**Figure 3-5**

*Land Use and Land Cover Map of Mekong River Basin (MRC, 2010)*



## 3.2 Data

### 3.2.1 In-situ River Discharge

In this study, in-situ data of daily discharge will be obtained from Mekong River Commission (MRC) (<https://mrcmekong.org/>) both for training and validation purposes. Eight locations on Mekong River will be used whose details is shown in Table 3-3 and is sorted according to the river's flow direction (1-8). These hydrological stations represent the different hydrological characteristics in the basin. These data will be used to develop a regional model. Further, last two gauge data (9-10) will be used to validate the predictive accuracy of regional model. The location of these stations is indicated in Figure 3-1.

**Table 3-3***List of in Situ Gauge Stations in the Mekong Mainstream used this Study*

S.N.	Name of Station	Station Code	Basin Coverage		Location		Streamflow Record
			km <sup>2</sup>	% Total	Latitude (°N)	Longitude (°E)	
1	Chiang Saen	TH_010501	199,008	21	20.273	100.083	Jan 1, 2002 to Dec 31, 2018*
2	Luang Prabang	LA_011201	288,380	31	19.892	102.137	
3	Vietiane	LA_011901	323,027	34	17.928	102.620	
4	Mukdahan	TH_013402	429,210	46	16.540	104.737	
5	Pakse	LA_013901	621,404	66	15.117	105.800	
6	Stung Treng	KH_014501	728,828	78	13.545	106.017	
7	Krati	KH_014901	747,958	80	12.240	105.987	
8	Tan Chau	VN_019803			10.803	105.243	
9	Jinghong	CN_092600			22.00	100.770	
10	Nakhon Phanom	TH_013101	373,000	47	17.40	104.800	

\*The period may vary based on data availability

### 3.2.2 Satellite Altimetry Data for Water Level

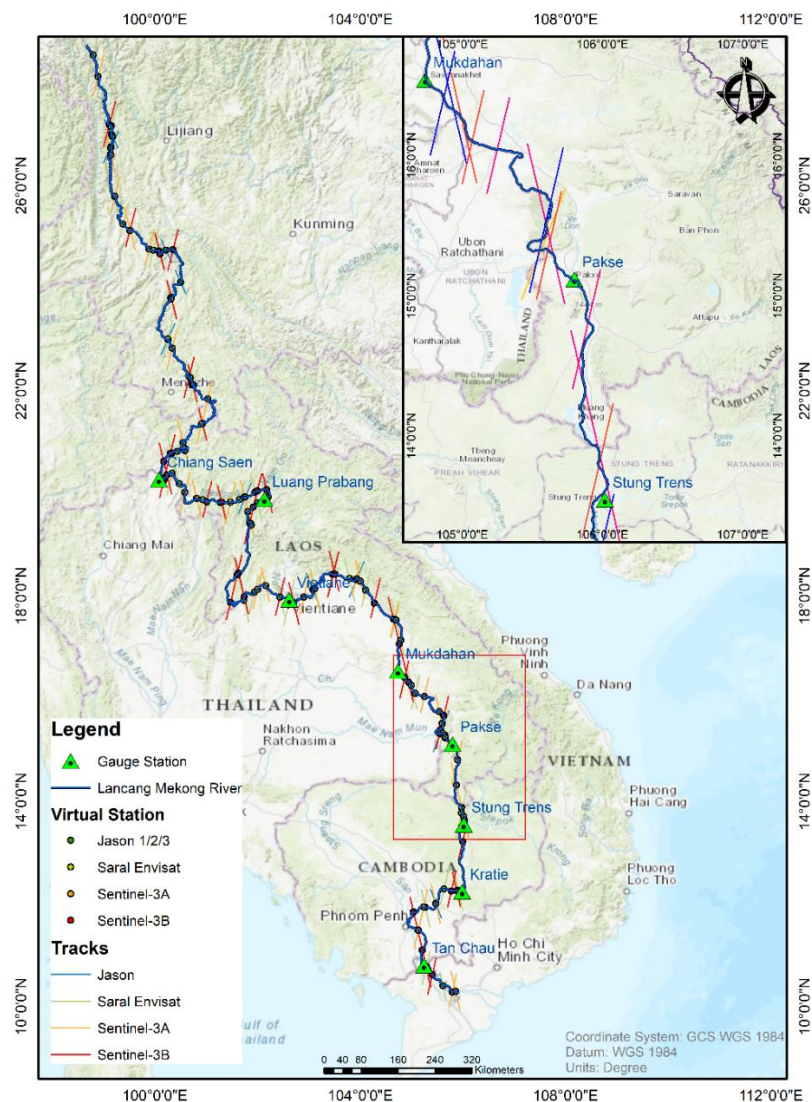
This study will use Envisat, Jason-1/2 and Sentinel-3A altimetry products to derive time series water level from 2002 to 2018 since these datasets are freely available by the service provider. Also, from these altimetry products, sufficient virtual stations can be located along the Lancang Mekong River. Figure 3-6 shows the altimeter tracks crossing Lancang Mekong River and Virtual Stations. Envisat provides data from 2002 to 2010 and has an orbital period of 35 days. The 18-Hz along-track range data in the Geophysical Data Record (GDR), which is publicly available from the Center for Topographic Studies of the Ocean and Hydrosphere (CTOH; <http://ctoh.legos.obs-mip.fr/data/alongtrack-data/datarequest>) will be used for Envisat.

Jason-1 and Jason-2 orbit at an altitude of 1336 km, with an inclination of 66°, on a 10-day repeat cycle, providing observations of the Earth surface (ocean and land) from 66° latitude North to 66° latitude South, with an equatorial ground-track spacing of about 315 km.

A collaboration between Centre National d'Etudes Spatiales (CNES) and the National Aeronautics and Space Administration (NASA) launched the Jason-1 mission on December 7th, 2001. The Jason-1 mission's sensors are based on the Poseidon-2 altimeter, a two-frequency altimeter with C (5.3 GHz) and Ku (13.575 GHz) bands that was part of the previous Topex/Poseidon missions. Along with the Jason Microwave Radiometer from NASA, the Doppler Orbitography and Radio-positioning Integrated by Satellite (DORIS) instrument from CNES, the Black Jack Global Positioning System receiver from NASA, and a Laser Retroreflector Array (LRA) from NASA/Jet Propulsion Laboratory (JPL) make up its payload, which allows for precise orbit determination. Jason-1 was decommissioned on June 21, 2013, and it stayed in its intended orbit until 26 January 2009.

**Figure 3-6**

*Virtual Stations Track along the Lancang Mekong River*





A collaboration between CNES, NASA, Exploitation of Meteorological Satellites (EUMETSAT), National Oceanic and Atmospheric Administration (NOAA) launched Jason-2 mission on June 20, 2008. The Advanced Microwave Radiometer (AMR) from JPL/NASA, the Global Navigation Satellite System (GNSS), and an LRA from JPL/NASA make up most of its payload, which also includes the real-time monitoring system DIODE of DORIS device from CNES, a GNSS transceiver from NASA/JPL, and the Poseidon-3 radar altimeter from CNES. Jason-2 remained in its nominal orbit until 3 July 2016.

European Space Agency (ESA) launched the Sentinel-3A mission on February 16, 2016, placing it in an 814-kilometer orbit. The satellite carries a single dual-frequency SAR altimeter named SRAL (SAR Radar Altimeter) (Ku-band at 13.575 GHz and C-band at 5.41 GHz). Additionally, its payload consists of a Microwave Radiometer (MWR) sensor for measuring wet path delays and a triple system for precisely determining orbits, which consists of a POD with a GPS receiver, an LRA, and a DORIS device. Table 3-4 provides the major characteristics of altimetry missions used in this study.

**Table 3-4**

*Major Features of the Radar Altimetry Missions used in this Study*

<b>Mission</b>	<b>Jason-1/2/3</b>	<b>ENVISAT</b>	<b>Sentinel-3A</b>
<b>Instrument</b>	Poseidon-2 Poseidon-3 Poseidon-3B	Radar Altimeter (RA-2)	Sar Radar Altimeter (SRAL)
<b>Space agency</b>	Centre National d'Etudes Spatiales (CNES) National Aeronautics and Space Administration (NASA)	European Space Agency (ESA)	European Space Agency (ESA)
<b>Operation</b>	2001–2013 Since 2008 Since 2016	2002–2012	Since 2016
<b>Acquisition mode</b>	Low Resolution Mode (LRM)	LRM	Pseudo Low Resolution Mode (PLRM), SAR

<b>Mission</b>	<b>Jason-1/2/3</b>	<b>ENVISAT</b>	<b>Sentinel-3A</b>
<b>Acquisition</b>	Along-track	Along-track	Along-track
<b>Frequency (GHz)</b>	13.575 (Ku) 5.3 (C)	13.8 (Ku) 13.575 (Ku) 3.2 (S)	13.575 (Ku) 5.41 (C)
<b>Altitude (km)</b>	1315	800	814.5
<b>Orbit inclination (°)</b>	66	98.55	98.65
<b>Repetitively (days)</b>	9.9156	35	27
<b>Equatorial cross-track separation (km)</b>	315	75	104

### ***3.2.3 Satellite Optical Data Sets***

The different satellite missions used in this study for the optical images are moderate-resolution imaging spectroradiometer (MODIS); MODIS AQUA and TERRA. Landsat data will be used to fill data gaps in MODIS based on data availability. Due to the coarse spatial resolution, MODIS has provided better results in large rivers with a width of more than 100 m for C/M estimation and thus selected for Mekong River. The optimal location for selecting wet pixel is the river area and inundation sensitive area during flood events ensuring minimum vegetation coverage while for dry pixel, area should be located far from river area preferably urban areas (Shi et al., 2020; Tarpanelli, Brocca, et al., 2013).

The MODIS is among the sensors on board the Earth Observing System (EOS) Terra (since 1999) and Aqua (since 2002) satellites. Due to its high temporal resolution of 1-2 days with occasionally two passes during a day at mid-latitude (3 h apart from each other), its moderate spatial resolution (2 channels at 250 m, 5 at 500 m, and 29 at 1 km), and its high spectral resolution of 36 bands ranging in wavelength from 0.4 m to 14.4 m, it is widely used for monitoring a variety of terrestrial, atmospheric, and ocean phenomena. This study uses level-2 products MOD09GQ and MYD09GQ from TERRA and AQUA, respectively, at daily resolution.

Landsat is a series of satellites that provide the longest temporal record of moderate resolution multispectral data of the earth’s surface on a global basis (40 years). The sensor on this satellite has a high spatial resolution, i.e., 30 m, but also a long grounding track repeat cycle of 15 days. Table 3-5 provides the major characteristics of optical satellite sensors used in this study.

**Table 3-5**

*Major Features of the Optical Satellite Sensors used in this Study*

<b>Optical Sensor</b>	<b>Product</b>	<b>Band (Spectral range in nm)</b>	<b>Temporal Resolution (days)</b>	<b>Spatial Resolution (m)</b>
MODIS AQUA	MYD09GQ	2 (841-876)	1-2	250
MODIS TERRA	MOD09GQ	2 (841-876)	1-2	250
LANDSAT	Landsat TM/ETM+	4 (772-898)	15	30

### **3.2.4 Basin Characteristics**

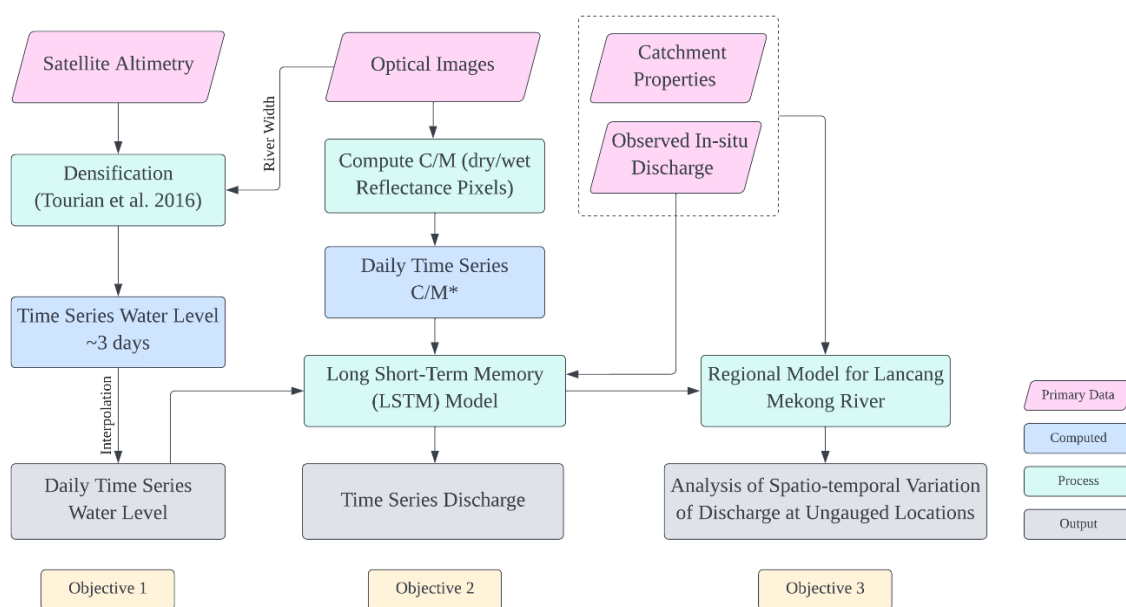
The characteristics of basin draining to each of the hydrological stations used in this study will be used as an input to ANN model while developing regional model. The parameters that will be used are catchment area, catchment centroid latitude, catchment centroid longitude, average catchment elevation, difference between highest and lowest elevated points in a catchment, average catchment slope, curve number and average mainstream bed slope gradient. The parameters will be computed from available DEM and land use data.

## CHAPTER 4 METHODOLOGY

The general procedure for river discharge estimation is shown in Figure 4-1. The details of the methodology are explained in this chapter. Long Short-Term Memory machine learning algorithm will be employed for estimating river discharge and will be evaluated. Further, regional model will be developed for Lancang Mekong River to study the spatio-temporal variation of river discharge at ungauged sites. The inputs to the model will be water level data obtained from satellite altimetry, reflectance ratio of dry and wet pixels from optical images and other catchment parameters. The performance of the model to simulate river discharge will be evaluated using different statistical indicators.

**Figure 4-1**

*Overall Methodological Framework for the study*

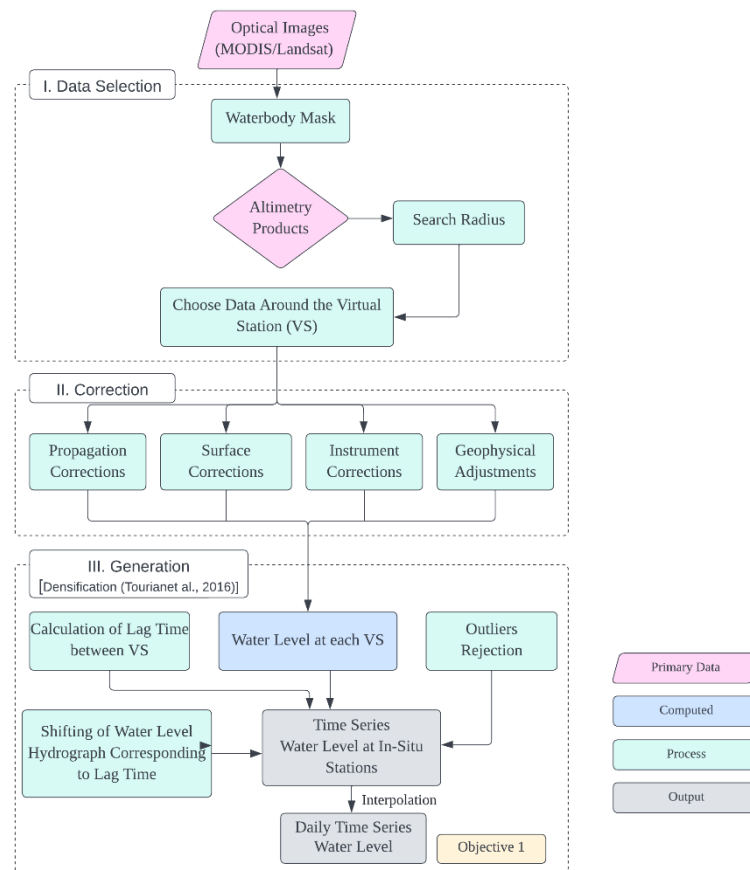


### 4.1 Estimation of water level at different stations in Mekong River

The methodological approach to estimate the water level at different reach of river using multi-mission satellite altimetry is shown in Figure 4-2.

**Figure 4-2**

*Methodological Approach to Estimate Water Level using Satellite Altimetry  
(Objective 1)*



#### **4.1.1 Time Series Water Level from Satellite Altimetry**

Particularly in inaccessible and complex areas, satellite remote sensing offers the exceptional opportunity to acquire freely accessible water level heights. Numerous altimetric missions, including TOPEX/Poseidon, Jason-1/2/3, ERS-1/2, Environmental Satellite (Envisat), CryoSat-2, SARAL/AltiKa, and Sentinel 3A, 3B, have contributed data over the past two decades that can be utilized to track the behavior of water bodies on Earth (Garkoti & Kundapura, 2021). The increased accuracy of the altimetry sensors encourages its use as a validation tool for many applications, from straightforward routing approaches to complex hydraulic models, and recent advancements in radar altimetry technology provide crucial information for river water level monitoring (Domeneghetti et al., 2015; Schneider et al., 2017).

The water surface level will be calculated from multiple satellite altimetry data at the corresponding time. Altimeter measurements of surface topography are distorted, and thus corrections will be applied. For example, atmospheric propagation effects in the

troposphere and the ionosphere, electromagnetic bias, residual geoid errors, and inverse barometer effects can all distort measurements (Sichangi et al., 2016). Considering propagation delays from the interactions of electromagnetic waves in the atmosphere and geophysical corrections, the height of the reflecting surface (H) with respect to a reference ellipsoid will be estimated. Thus, the types of corrections to be applied are geophysical corrections for wet troposphere, dry troposphere, ionosphere, solid earth tides and pole tides. The accuracy of obtained water level will be evaluated comparing with in-situ water level for available locations.

#### ***4.1.2 Densification of Altimetry derived Time Series Water Level at In-situ Stations***

Multi-mission altimetry products will be used to increase the temporal resolution of water level in this study. The time series water level will be derived at various Virtual Stations (VS) from different satellite missions. The water level obtained from different satellite mission will have bias within due to mission's geophysical data and these intersatellite bias will be estimated and removed and other errors of the altimetry data will be corrected as mentioned. Then, the Virtual Stations (VS) will be connected hydraulically and statistically using an algorithm developed by (Tourian et al., 2016, 2017) using the time series water level data, river width and slope. For this, time lag between virtual stations needs to be estimated.

The time lag between VSs will be determined using the anticipated river width and the slope obtained from satellite altimetry using the Equation 4-1.

$$T_L = \frac{L}{c} = \frac{L}{bV} \quad \text{Equation 4-1}$$

Where,  $T_L$  is travel time, L is the distance between the virtual stations, c is celerity,  $b = \text{constant} = 5/3$  and V is the velocity. The velocity is computed by the Equation 4-2 developed by (Tourian et al., 2016).

$$V = 1.48W^{-0.8}S^{0.6} \quad \text{Equation 4-2}$$

where, W refers to river width and S is the slope of the river.

Then, at any location along the river, integration of all the altimetric readings will be done by stacking all the obtained altimetric measurements at a reference location by shifting the water level hydrographs of all virtual stations according to corresponding

time lag. The measurement will be merged by normalizing the time series in accordance with their statistical properties. The readings will be rescaled down to their actual water level values after an outlier identification procedure.

### **River Width Estimation:**

Google Earth Engine (GEE) based river width algorithm RivWidthCloud developed by Yang et al. (2020) will be used to extract river centerline and width from remotely sensed images. The simplicity of usage based on a well-liked cloud computing environment GEE and the flagging power to automatically reduce negative impact from cloud and shadows are two key advantages of RivWidthCloud over previous river width measuring techniques. These benefits spare users the expense of downloading, storing, and locally processing remote sensing data, enabling them to easily extract common width statistics and time series.

Firstly, extraction of river mask from satellite image will be done. Then, river centerline from the river mask will be derived and river width along the centerline will be obtained at each river section. To calculate the river width, for each centerline pixel the direction orthogonal to the local centerline is computed at first and then river width along these orthogonal directions is computed. The extracted centerline will also be used to define the along-river coordinate distance between Virtual Station (VS)s and to compute the slope.

## **4.2 Daily discharge estimation by merging satellite optical and altimetry data**

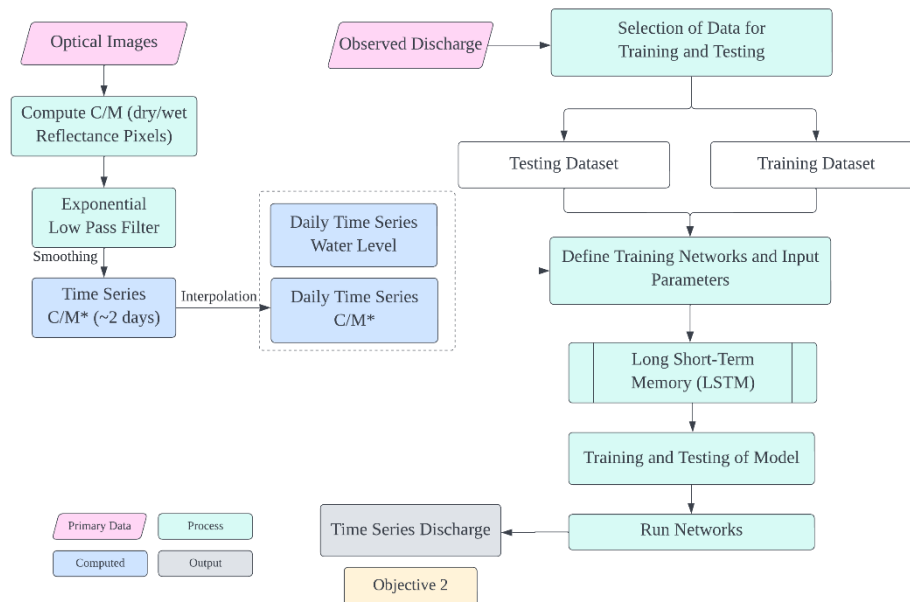
The methodological framework to accomplish this objective is shown in Figure 4-3.

The surface reflectance between water and land from Near Infra-Red (NIR) band of optical sensors will have different pixel values. The water pixel (M) has lower reflectance than land pixel (C) in which reflectance value of water pixel decreases with flooding events while land pixel doesn't vary much and assumed to be constant (Tarpanelli et al., 2017). Thus, measuring time series variation in reflectance of water pixel with respect to land pixel helps to provide variation in river discharge indirectly. The ratio between the spectral reflectance of the C and M pixels should theoretically allow a minimizing of the atmospheric effects because disturbances derived from the atmosphere influence both C and M in the same way (Tarpanelli, Brocca, et al., 2013).

The values of C/M increase with the presence of water and, hence, with discharge. Hence, ratio of C and M is taken as the proxy for measurement of river discharge.

**Figure 4-3**

*Methodological Framework for Discharge Estimation Merging Optical Sensor Data and Altimetry Data (Objective 2)*



A cloudy sky, on the other hand, renders the optical pictures useless and causes data outages in the measurements. Also, the selected location of C and M pixels may also affect the accuracy of discharge estimation. The data from more satellite missions of the same kind might be gathered and combined to provide the necessary information as a feasible solution in these circumstances. Thus, this study uses an Artificial Neural Network (ANN) approach to combine observations from optical sensors with altimetry data for estimation of river discharge to overcome these issues.

#### 4.2.1 C/M from Satellite Optical Data Sets

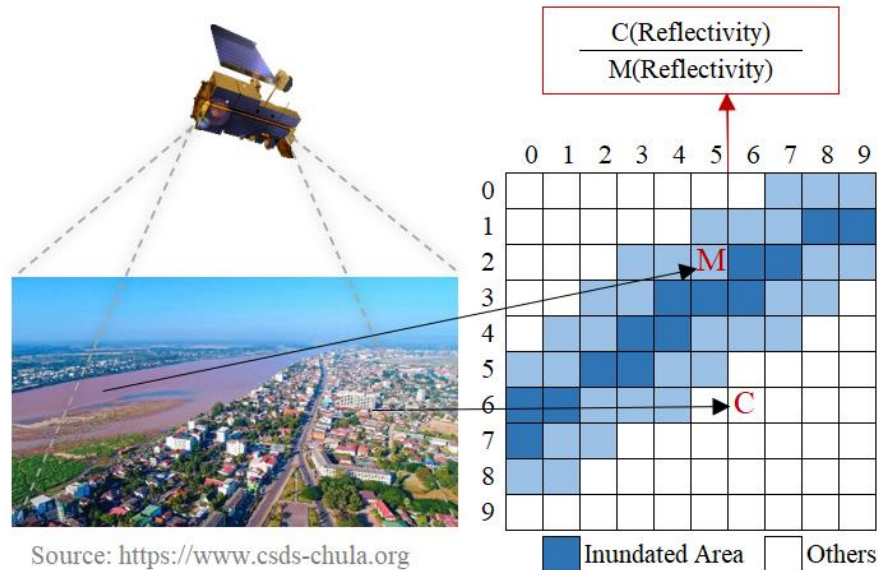
The ratio of the surface reflectance of a land pixel named C (calibration), situated close to the river in an area free of surface water even during high flooding, and of a water pixel named M (measurement), situated within the river with the permanent presence of water, will be computed. Figure 4-4 shows the typical representation of wet and dry pixel reflectivity. First, the cloud-affected pixels will be located and eliminated. Then, the location for selecting M and C pixels will be chosen. The optimal site for wet pixel M is next to a river in a region that is both entirely submerged in water and sensitive to



changes in the flooded area during flood occurrences. The calibration's dry pixel C is situated outside the river, above urban areas that are not impacted by the seasonal cycle of vegetation, and in places that are not surrounded by water.

**Figure 4-4**

*A representation of wet and dry pixel reflectivity*



To create a time series of C/M, multiple images for the study period will be evaluated. Then, to reduce the noise effects due to atmospheric contribution, time series of C/M will be smoothed with a low pass filter (averaging moving window) to get C/M\*.

#### **4.2.2 Merging Multiple Satellite Datasets**

All the datasets should have common time series for successful merging of different data from various sources. While the water level altimetry time series is restricted to the passage of satellites over the river, the C/M\* ratio retrieved from optical satellite sensors is impacted by cloudy images. These circumstances result in missing data, which breaks up the time series. In addition, the accuracy of the altimetry multi-mission satellites might vary based on the altimeter utilized and the number of satellites available at the same time. Due to the satellites' repetition cycle, the time series generated by optical sensors have different temporal resolutions. When compared to altimetric time series, MODIS-derived time series have a better temporal resolution. The expected temporal resolution of altimetry data is approximately 3 to 5 days and MODIS-derived data is approximately 2 to 3 days.

Therefore, to overcome this issue, all satellite data sets will be interpolated at the daily scale to provide time series with the same frequency that are consistent with the temporal resolution of ground observations. Daily data gaps will be linearly filled up by interpolating values between the closest previous and next values.

The ANN methodology will be used to carry out the merging process. With this method, data from many sources can be combined into a single retrieval strategy by simply adding or removing inputs from the ANN configuration and updating the training accordingly. The daily data sets function the inputs to the ANN: river water level and C/M\*. For modeling, Long Short-Term Memory (LSTM) ANN model will be employed. The number of hidden layers and hidden neurons will be established by trial-and-error procedure. The training set and validation set will be sampled randomly.

### **Long Short-Term Memory (LSTM):**

LSTM networks are specifically designed to learn long-term dependencies and can overcome the problems of vanishing and exploding gradients. LSTM networks are composed of an input layer, one or more memory cells, and an output layer (Zebin et al., 2018). The number of neurons in the input layer is equal to the number of explanatory variables. The main characteristic of LSTM networks is contained in the hidden layer consisting of so-called memory cells. Each of the memory cells has three gates maintaining and adjusting its cell state  $s_t$ : a forget gate ( $f_t$ ), an input gate ( $i_t$ ), and an output gate ( $o_t$ ).

At every time-step  $t$ , each of the three gates is presented with the input  $x_t$  (one element of the) as well as the output  $h_{t-1}$  of the memory cells at the previous time-step  $t-1$ . Hereby, the gates act as filters, each fulfilling a different purpose:

- The forget gate defines what information is removed from the cell state.
- The input gate specifies what information is added to the cell state.
- The output gate specifies what information from the cell state is used

Each of the gates has parameters for its weights and biases, giving many parameters for deep networks with many units' present. The weights of these connections are learned or updated during the training of the network.

### 4.2.3 Evaluation of the performance of Long Short-Term Memory (LSTM) Model

The performances of the LSTM model to simulate discharge at various sites of Lancang Mekong River will be evaluated based on the coefficient of determination ( $R^2$ ), root mean square error (RMSE) and percent bias (PBIAS), and visual interpretation using a line diagram and scatter diagram. This will be done by comparing the observed discharge at in-situ stations with simulated discharge.

$$R^2 = \frac{n \sum Q_i^{obs} Q_i^{pre} - \sum Q_i^{obs} \sum Q_i^{pre}}{(\sqrt{n \sum Q_i^{obs}{}^2 - (\sum Q_i^{obs})^2}) * (\sqrt{n \sum Q_i^{pre}{}^2 - (\sum Q_i^{pre})^2})} \quad \text{Equation 4-3}$$

$$RMSE = \sqrt{\frac{\sum_{i=1}^n (Q_i^{obs} - Q_i^{pre})^2}{N}} \quad \text{Equation 4-4}$$

$$PBIAS = \frac{\sum_{i=1}^n (Q_i^{obs} - Q_i^{pre}) * 100}{\sum_{i=1}^n (Q_i^{obs})} \quad \text{Equation 4-5}$$

where,  $Q_i^{obs}$  is observed discharge,  $Q_i^{pre}$  is predicted discharge and  $\bar{Q}_i^{obs}$  is the average observed discharge.

#### **Coefficient of Determination ( $R^2$ ):**

The coefficient of determination describes the statistical relationship between the variables and helps to show the nature of association among the predicted and observed data.  $R^2$  is the ratio of explained variation compared to the total variation. It ranges from 0 to 1; its higher value indicates less error variance, and generally, a value greater than 0.5 is considered acceptable. This statistical tool is highly sensitive to outliers and insensitive to additive and proportional differences between observed and predicted data.

#### **Root Mean Square Error (RMSE):**

The square root of the average square of all the errors is called root mean square error (RMSE). It is an excellent general-purpose error matrix commonly used for the numerical prediction model. RMSE has a good measure of accuracy, but it can only compare the prediction error of models or configure a particular variable and not between two different variables, making it scalar-dependent. RMSE lies between 0 to  $\infty$ .

### Percent Bias (PBIAS):

Percent bias measures the relationship between the observed data and its predicted data; it measures the average tendency of observed data to be larger or smaller than the predicted data. Percent bias describes whether the simulated model is overestimated or underestimated. A low PBIAS value or a value that tends to zero indicates the optimal model. A negative value indicates the overestimation of the model. In contrast, a positive PBIAS value indicates an underestimation of the model. When the data are evaluated, PBIAS reveals any deviation of the data as a percentage.

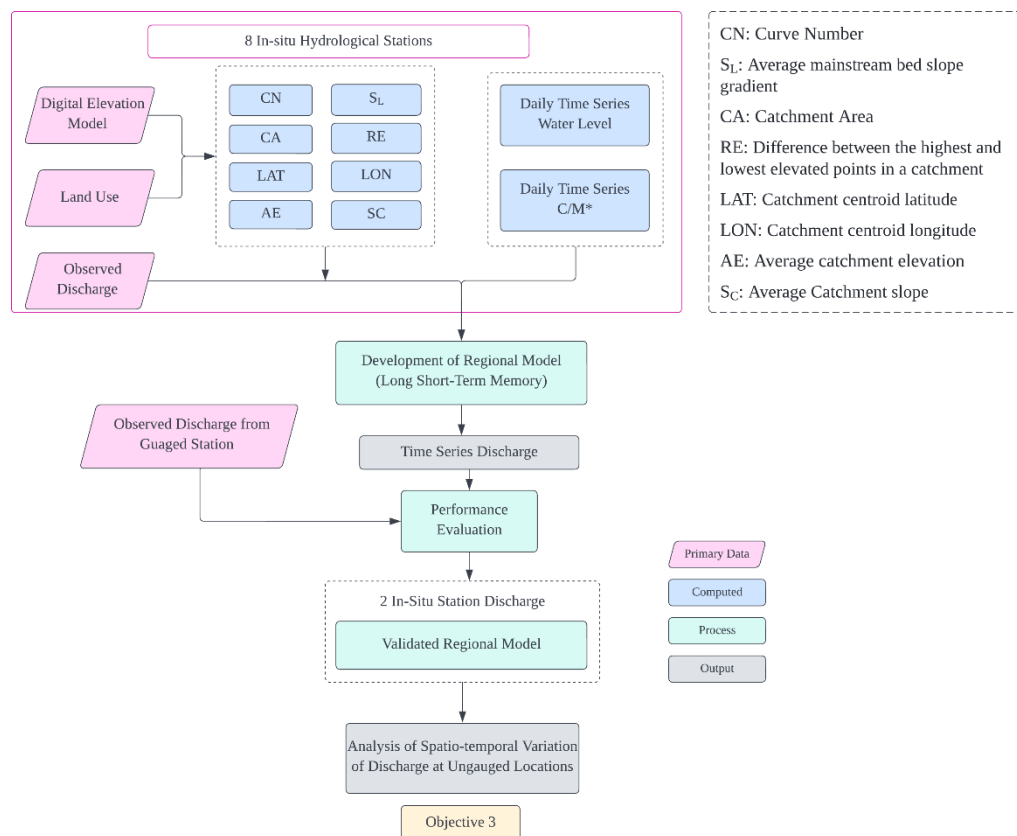
A model with higher  $R^2$  and NSE values, and lower RMSE and PBAIS values, decres a relatively better model for the simulation of discharge.

### 4.3 Development of a regional model for estimation of the river discharge

The methodological framework to achieve this objective is presented in Figure 4-5.

**Figure 4-5**

*Methodological Framework for Development of Regional Model for Discharge Estimation (Objective 3)*



There are limited number of hydrological gauging stations in Mekong River, and it is not always feasible to measure discharge at every location in the river reach. On other hand, it is not always easy to obtain gauge data due to various reasons. However, developing regional model considering parameters obtained from remote sensing and catchment characteristics for entire basin will help to predict discharge at any required location without physically being present. The initial lists of catchment parameters that are expected to have impact on discharge are provided in Table 4-1. Sensitivity analysis of these parameters will be carried out to obtain most sensitive parameters that will have profound effect on discharge and final catchment parameters will be obtained.

Then, a regional model will be established by integrating the catchment parameters along with time series water level and C/M\* for eight in-situ stations within the river reach. This model could then be applied simply but with strong predictive power to estimate catchment-scale discharge in ungauged reach of Lancang Mekong River. Physical catchment descriptors and model parameters are known to be interdependent. Also, it is well known that their interactions are highly nonlinear; therefore, ANN can be a suitable tool for the regionalization of model parameters (Soni et al., 2021). Thus, the integration will be done using the best selected machine learning approach from Section 4.2.3. The performance of regional model will be tested against other two gauged hydrological stations to check the predictive accuracy using the statistical indicators.

**Table 4-1**

*Basin attributes and parameters used for regionalization*

<b>S.N.</b>	<b>Parameters</b>	<b>Acronym</b>	<b>Remarks</b>
1	Catchment Area	CA	
2	Catchment centroid latitude	LAT	
3	Catchment centroid longitude	LON	
4	Average catchment elevation	AE	
5	Difference between the highest and lowest elevated points in a catchment	RE	
6	Average Catchment slope	Sc	
7	Curve Number	CN	
8	Average mainstream bed slope gradient	SL	

## **CHAPTER 5**

### **EXPECTED OUTPUTS**

The following outputs are anticipated after the successful completion of proposed study:

1. Water level and discharge at different gauged locations in Mekong River using remote sensing.
2. A developed regional model for Lancang Mekong River Basin to estimate river discharge at ungauged sites.
3. Spatial and temporal variation of river discharge at ungauged reach of Lancang Mekong River.



**CHAPTER 7**  
**PROPOSED BUDGET**

The proposed budget for the study is presented in Table 7-1:

**Table 7-1**

*Proposed Budget for the Study*

S.N.	Description	Estimated Cost (Thai Baht)	Remarks
<b>1</b>	<b>Data Acquisition</b>		
1.1	Hydrological Data	2500	
1.2	Remote Sensing Data	3000	
	<b>Sub Total</b>	<b>5500</b>	
<b>2</b>	<b>Transportation</b>		
2.1	Taxi	2500	
2.2	Local Transportation	1000	
	<b>Sub Total</b>	<b>3500</b>	
<b>3</b>	<b>Purchase of Online Resources</b>		
3.1	Student License for ArcGIS	4000	
3.2	Course on R/Python	1500	
3.3	Course on Remote Sensing	3000	
3.4	Course on Machine Learning	2500	
	<b>Sub Total</b>	<b>11000</b>	
<b>4</b>	<b>Miscellaneous</b>		
4.1	Telephone/Internet	3000	
4.2	Reports/Documents	1000	
4.3	Photocopy	500	
4.4	SSD Upgrade	8000	
	<b>Sub Total</b>	<b>12500</b>	
<b>5</b>	<b>Report Preparation</b>		
5.1	Report Printing	4000	
5.2	Photocopy and Binding	2000	
	<b>Sub Total</b>	<b>6000</b>	
<b>6</b>	<b>Contingency</b>	<b>5000</b>	
	<b>Grand Total (1+2+3+4+5+6)</b>	<b>43500</b>	



## REFERENCES

- Ahn, J.-H., & Park, Y.-J. (2020). Estimating Water Reflectance at Near-Infrared Wavelengths for Turbid Water Atmospheric Correction: A Preliminary Study for GOCI-II. *Remote Sensing*, *12*(22), 3791. <https://doi.org/10.3390/rs12223791>
- Arnell, N. W., & Gosling, S. N. (2013). The impacts of climate change on river flow regimes at the global scale. *Journal of Hydrology*, *486*, 351–364. <https://doi.org/10.1016/j.jhydrol.2013.02.010>
- Bengio, Y. (2009). Learning Deep Architectures for AI. *Foundations and Trends® in Machine Learning*, *2*(1), 1–127. <https://doi.org/10.1561/22000000006>
- Biancamaria, S., Andreadis, K. M., Durand, M., Clark, E. A., Rodriguez, E., Mognard, N. M., Alsdorf, D. E., Lettenmaier, D. P., & Oudin, Y. (2010). Preliminary Characterization of SWOT Hydrology Error Budget and Global Capabilities. *IEEE Journal of Selected Topics in Applied Earth Observations and Remote Sensing*, *3*(1), 6–19. <https://doi.org/10.1109/JSTARS.2009.2034614>
- Biancamaria, S., Frappart, F., Leleu, A.-S., Marieu, V., Blumstein, D., Desjonquères, J.-D., Boy, F., Sottolichio, A., & Valle-Levinson, A. (2017). Satellite radar altimetry water elevations performance over a 200m wide river: Evaluation over the Garonne River. *Advances in Space Research*, *59*(1), 128–146. <https://doi.org/10.1016/j.asr.2016.10.008>
- Birkinshaw, S. J., Moore, P., Kilsby, C. G., O'Donnell, G. M., Hardy, A. J., & Berry, P. A. M. (2014). Daily discharge estimation at ungauged river sites using remote sensing: DAILY DISCHARGE ESTIMATION USING REMOTE SENSING. *Hydrological Processes*, *28*(3), 1043–1054. <https://doi.org/10.1002/hyp.9647>
- Birkinshaw, S. J., O'Donnell, G. M., Moore, P., Kilsby, C. G., Fowler, H. J., & Berry, P. A. M. (2010). Using satellite altimetry data to augment flow estimation techniques on the Mekong River. *Hydrological Processes*, *24*(26), 3811–3825. <https://doi.org/10.1002/hyp.7811>
- Bjerklie, D. M., Birkett, C. M., Jones, J. W., Carabajal, C., Rover, J. A., Fulton, J. W., & Garambois, P.-A. (2018). Satellite remote sensing estimation of river discharge: Application to the Yukon River Alaska. *Journal of Hydrology*, *561*, 1000–1018. <https://doi.org/10.1016/j.jhydrol.2018.04.005>
- Bjerklie, D. M., Lawrence Dingman, S., Vorosmarty, C. J., Bolster, C. H., & Congalton, R. G. (2003). Evaluating the potential for measuring river discharge from space. *Journal of Hydrology*, *278*(1–4), 17–38. [https://doi.org/10.1016/S0022-1694\(03\)00129-X](https://doi.org/10.1016/S0022-1694(03)00129-X)
- Bjerklie, D. M., Moller, D., Smith, L. C., & Dingman, S. L. (2005). Estimating discharge in rivers using remotely sensed hydraulic information. *Journal of Hydrology*, *309*(1–4), 191–209. <https://doi.org/10.1016/j.jhydrol.2004.11.022>

- Bogning, S., Frappart, F., Blarel, F., Niño, F., Mahé, G., Bricquet, J.-P., Seyler, F., Onguéné, R., Etamé, J., Paiz, M.-C., & Braun, J.-J. (2018). Monitoring Water Levels and Discharges Using Radar Altimetry in an Ungauged River Basin: The Case of the Ogooué. *Remote Sensing*, *10*(2), 350. <https://doi.org/10.3390/rs10020350>
- Brakenridge, G. R., Nghiem, S. V., Anderson, E., & Chien, S. (2005). Space-based measurement of river runoff. *Eos, Transactions American Geophysical Union*, *86*(19), 185–188. <https://doi.org/10.1029/2005EO190001>
- Brakenridge, G. R., Nghiem, S. V., Anderson, E., & Mic, R. (2007). Orbital microwave measurement of river discharge and ice status. *Water Resources Research*, *43*(4). <https://doi.org/10.1029/2006WR005238>
- Brakenridge, r., & anderson, e. (2006). Modis-based flood detection, mapping and measurement: the potential for operational hydrological applications. In J. Marsalek, G. Stancalie, & G. Balint (Eds.), *Transboundary Floods: Reducing Risks Through Flood Management* (pp. 1–12). Springer Netherlands. [https://doi.org/10.1007/1-4020-4902-1\\_1](https://doi.org/10.1007/1-4020-4902-1_1)
- Calmant, S., & Seyler, F. (2006). Continental surface waters from satellite altimetry. *Comptes Rendus Geoscience*, *338*(14–15), 1113–1122. <https://doi.org/10.1016/j.crte.2006.05.012>
- Camps-Valls, G. (2009). Machine learning in remote sensing data processing. *2009 IEEE International Workshop on Machine Learning for Signal Processing*, 1–6. <https://doi.org/10.1109/MLSP.2009.5306233>
- Cheng, S., Qiao, X., Shi, Y., & Wang, D. (2021). Machine learning for predicting discharge fluctuation of a karst spring in North China. *Acta Geophysica*, *69*(1), 257–270. <https://doi.org/10.1007/s11600-020-00522-0>
- Chiang, Y.-M., Hao, R.-N., Zhang, J.-Q., Lin, Y.-T., & Tsai, W.-P. (2018). Identifying the Sensitivity of Ensemble Streamflow Prediction by Artificial Intelligence. *Water*, *10*(10), 1341. <https://doi.org/10.3390/w10101341>
- Depetris, P. J. (2021). The Importance of Monitoring River Water Discharge. *Frontiers in Water*, *3*. <https://www.frontiersin.org/articles/10.3389/frwa.2021.745912>
- Derecki, J. A., & Quinn, F. H. (1987). Use of current meters for continuous measurement of flows in large rivers. *Water Resources Research*, *23*(9), 1751–1756. <https://doi.org/10.1029/WR023i009p01751>
- Dingman, S. L., & Bjerklie, D. M. (2005). Estimation of River Discharge. In M. G. Anderson & J. J. McDonnell (Eds.), *Encyclopedia of Hydrological Sciences* (p. hsa069). John Wiley & Sons, Ltd. <https://doi.org/10.1002/0470848944.hsa069>
- Domeneghetti, A., Castellarin, A., Tarpanelli, A., & Moramarco, T. (2015). Investigating the uncertainty of satellite altimetry products for hydrodynamic modelling. *Hydrological Processes*, *29*(23), 4908–4918. <https://doi.org/10.1002/hyp.10507>

- Elumalai, V., Brindha, K., Sithole, B., & Lakshmanan, E. (2017). Spatial interpolation methods and geostatistics for mapping groundwater contamination in a coastal area. *Environmental Science and Pollution Research*, 24(12), 11601–11617. <https://doi.org/10.1007/s11356-017-8681-6>
- Esmaeilzadeh, B., Sattari, M. T., & Samadianfard, S. (2017). Performance evaluation of ANNs and an M5 model tree in Sattarkhan Reservoir inflow prediction. *ISH Journal of Hydraulic Engineering*, 23(3), 283–292. <https://doi.org/10.1080/09715010.2017.1308277>
- Fekete, B. M., & Vörösmarty, C. J. (2007). *The current status of global river discharge monitoring and potential new technologies complementing traditional discharge measurements*. 8.
- Filippucci, P., Brocca, L., Bonafoni, S., & Tarpanelli, A. (2022). *River Discharge estimation from optical satellite data: Latest advances using NIR sensors* [Other]. display. <https://doi.org/10.5194/egusphere-egu22-3513>
- Florkowski, T., Davis, T. G., Wallander, B., & Prabhakar, D. R. L. (1969). The measurement of high discharges in turbulent rivers using tritium tracer. *Journal of Hydrology*, 8(3), 249–264. [https://doi.org/10.1016/0022-1694\(69\)90001-8](https://doi.org/10.1016/0022-1694(69)90001-8)
- Frappart, F., Blumstein, D., Cazenave, A., Ramillien, G., Birol, F., Morrow, R., & Rémy, F. (2017). Satellite Altimetry: Principles and Applications in Earth Sciences. In J. G. Webster, *Wiley Encyclopedia of Electrical and Electronics Engineering* (pp. 1–25). John Wiley & Sons, Inc. <https://doi.org/10.1002/047134608X.W1125.pub2>
- Frappart, F., Papa, F., Silva, J. S. da, Ramillien, G., Prigent, C., Seyler, F., & Calmant, S. (2012). Surface freshwater storage and dynamics in the Amazon basin during the 2005 exceptional drought. *Environmental Research Letters*, 7(4), 044010. <https://doi.org/10.1088/1748-9326/7/4/044010>
- Garkoti, A., & Kundapura, S. (2021). Deriving water level and discharge estimation using satellite altimetry for Krishna River, Karnataka. *Remote Sensing Applications: Society and Environment*, 22, 100487. <https://doi.org/10.1016/j.rsase.2021.100487>
- Ghumman, A. R., Ghazaw, Y. M., Sohail, A. R., & Watanabe, K. (2011). Runoff forecasting by artificial neural network and conventional model. *Alexandria Engineering Journal*, 50(4), 345–350. <https://doi.org/10.1016/j.aej.2012.01.005>
- Gleason, C., & Durand, M. (2020). Remote Sensing of River Discharge: A Review and a Framing for the Discipline. *Remote Sensing*, 12(7), 1107. <https://doi.org/10.3390/rs12071107>
- Gravelle, R. (2015). *Discharge Estimation: Techniques and Equipment*.
- GRDC Data Portal. (2022). Retrieved June 16, 2022, from <https://portal.grdc.bafg.de/applications/public.html?publicuser=PublicUser#dataDownload/Home>

- Greff, K., Srivastava, R. K., Koutník, J., Steunebrink, B. R., & Schmidhuber, J. (2017). LSTM: A Search Space Odyssey. *IEEE Transactions on Neural Networks and Learning Systems*, 28(10), 2222–2232. <https://doi.org/10.1109/TNNLS.2016.2582924>
- He, D., Lu, Y., & Li, Z. *Chapter 14—Watercourse Environmental Change in Upper Mekong*. 28.
- Hirsch, R. M., & Costa, J. E. (2004). U.S. stream flow measurement and data dissemination improve. *Eos, Transactions American Geophysical Union*, 85(20), 197–203. <https://doi.org/10.1029/2004EO200002>
- Hoang, L. P., Lauri, H., Kumm, M., Koponen, J., van Vliet, M. T. H., Supit, I., Leemans, R., Kabat, P., & Ludwig, F. (2016). Mekong River flow and hydrological extremes under climate change. *Hydrology and Earth System Sciences*, 20(7), 3027–3041. <https://doi.org/10.5194/hess-20-3027-2016>
- Hochreiter, S., & Schmidhuber, J. (1997). Long Short-Term Memory. *Neural Computation*, 9(8), 1735–1780. <https://doi.org/10.1162/neco.1997.9.8.1735>
- Hou, J., van Dijk, A. I. J. M., Renzullo, L. J., & Vertessy, R. A. (2018). Using modelled discharge to develop satellite-based river gauging: A case study for the Amazon Basin. *Hydrology and Earth System Sciences*, 22(12), 6435–6448. <https://doi.org/10.5194/hess-22-6435-2018>
- Hu, C., Wu, Q., Li, H., Jian, S., Li, N., & Lou, Z. (2018). Deep Learning with a Long Short-Term Memory Networks Approach for Rainfall-Runoff Simulation. *Water*, 10(11), 1543. <https://doi.org/10.3390/w10111543>
- Huang, Q., Long, D., Du, M., Zeng, C., Qiao, G., Li, X., Hou, A., & Hong, Y. (2018). Discharge estimation in high-mountain regions with improved methods using multisource remote sensing: A case study of the Upper Brahmaputra River. *Remote Sensing of Environment*, 219, 115–134. <https://doi.org/10.1016/j.rse.2018.10.008>
- Jiang, L., Schneider, R., Andersen, O., & Bauer-Gottwein, P. (2017). CryoSat-2 Altimetry Applications over Rivers and Lakes. *Water*, 9, 211. <https://doi.org/10.3390/w9030211>
- Kao, I.-F., Zhou, Y., Chang, L.-C., & Chang, F.-J. (2020). Exploring a Long Short-Term Memory based Encoder-Decoder framework for multi-step-ahead flood forecasting. *Journal of Hydrology*, 583, 124631. <https://doi.org/10.1016/j.jhydrol.2020.124631>
- Kashid, S. G., & Pardeshi, S. A. (2014). A survey of water distribution system and new approach to intelligent water distribution system. *2014 First International Conference on Networks & Soft Computing (ICNSC2014)*, 339–344. <https://doi.org/10.1109/CNSC.2014.6906645>
- Kenny, J. F., Barber, N. L., Hutson, S. S., Linsey, K. S., Lovelace, J. K., & Maupin, M. A. (2009). *Estimated use of water in the United States in 2005* (Report No. 1344; Circular, p. 60). USGS Publications Warehouse. <https://doi.org/10.3133/cir1344>

- Kim, Lee, Chang, Bui, Jayasinghe, Basnayake, Chishtie, & Hwang. (2019). Daily River Discharge Estimation Using Multi-Mission Radar Altimetry Data and Ensemble Learning Regression in the Lower Mekong River Basin. *Remote Sensing*, 11(22), 2684. <https://doi.org/10.3390/rs11222684>
- Kim, Y., Schmid, T., Charbiwala, Z. M., Friedman, J., & Srivastava, M. B. (2008). NAWMS: Nonintrusive autonomous water monitoring system. *Proceedings of the 6th ACM Conference on Embedded Network Sensor Systems - SenSys '08*, 309. <https://doi.org/10.1145/1460412.1460443>
- Kouraev, A. V., Zakharova, E. A., Samain, O., Mognard, N. M., & Cazenave, A. (2004). Ob' river discharge from TOPEX/Poseidon satellite altimetry (1992–2002). *Remote Sensing of Environment*, 93(1), 238–245. <https://doi.org/10.1016/j.rse.2004.07.007>
- Kratzert, F., Klotz, D., Brenner, C., Schulz, K., & Herrnegger, M. (2018). *Rainfall-Runoff modelling using Long-Short-Term-Memory (LSTM) networks* [Preprint]. Catchment hydrology/Modelling approaches. <https://doi.org/10.5194/hess-2018-247>
- Leon, J. G., Calmant, S., Seyler, F., Bonnet, M.-P., Cauhopé, M., Frappart, F., Filizola, N., & Fraizy, P. (2006). Rating curves and estimation of average water depth at the upper Negro River based on satellite altimeter data and modeled discharges. *Journal of Hydrology*, 328(3), 481–496. <https://doi.org/10.1016/j.jhydrol.2005.12.006>
- Li, H., Li, H., Wang, J., & Hao, X. (2019). Extending the Ability of Near-Infrared Images to Monitor Small River Discharge on the Northeastern Tibetan Plateau. *Water Resources Research*, 55(11), 8404–8421. <https://doi.org/10.1029/2018WR023808>
- Lin, P., Pan, M., Beck, H. E., Yang, Y., Yamazaki, D., Frasson, R., David, C. H., Durand, M., Pavelsky, T. M., Allen, G. H., Gleason, C. J., & Wood, E. F. (2019). Global Reconstruction of Naturalized River Flows at 2.94 Million Reaches. *Water Resources Research*, 55(8), 6499–6516. <https://doi.org/10.1029/2019WR025287>
- Liu, K.-T., Tseng, K.-H., Shum, C., Liu, C.-Y., Kuo, C.-Y., Liu, G., Jia, Y., & Shang, K. (2016). Assessment of the Impact of Reservoirs in the Upper Mekong River Using Satellite Radar Altimetry and Remote Sensing Imageries. *Remote Sensing*, 8(5), 367. <https://doi.org/10.3390/rs8050367>
- Mekong River Commission. (2010). State of the Basin Report 2010. Mekong River Commission, Vientiane, Lao PDR.
- Mekong River Commission. (2019). State of the Basin Report 2018. Mekong River Commission, Vientiane, Lao PDR.
- Mekong River Commission. (2021). The integrated water resources management–based Basin Development Strategy for the Lower Mekong Basin 2021–2030 and the MRC Strategic Plan 2021–2025. Vientiane: MRC Secretariat.
- Mengen, D., Ottinger, M., Leinenkugel, P., & Ribbe, L. (2020). Modeling River Discharge Using Automated River Width Measurements Derived from Sentinel-1 Time Series. *Remote Sensing*, 12(19), 3236. <https://doi.org/10.3390/rs12193236>

- Milliman, J. D., & Farnsworth, K. L. (2011). *River Discharge to the Coastal Ocean: A Global Synthesis* (1st ed.). Cambridge University Press. <https://doi.org/10.1017/CBO9780511781247>
- MODIS Web. (2022). Retrieved July 30, 2022, from <https://modis.gsfc.nasa.gov/data/>
- Nogueira Filho, F. J. M., Souza Filho, F. de A., Porto, V. C., Vieira Rocha, R., Sousa Estácio, Á. B., & Martins, E. S. P. R. (2022). Deep Learning for Streamflow Regionalization for Ungauged Basins: Application of Long-Short-Term-Memory Cells in Semiarid Regions. *Water*, *14*(9), 1318. <https://doi.org/10.3390/w14091318>
- Ordóñez, F. J., & Roggen, D. (2016). Deep Convolutional and LSTM Recurrent Neural Networks for Multimodal Wearable Activity Recognition. *Sensors*, *16*(1), 115. <https://doi.org/10.3390/s16010115>
- Pan, F. (2013). Remote sensing of river stage and discharge. *SPIE Newsroom*. <https://doi.org/10.1117/2.1201212.004611>
- Papa, F., Durand, F., Rossow, W. B., Rahman, A., & Bala, S. K. (2010). Satellite altimeter-derived monthly discharge of the Ganga-Brahmaputra River and its seasonal to interannual variations from 1993 to 2008. *Journal of Geophysical Research: Oceans*, *115*(C12). <https://doi.org/10.1029/2009JC006075>
- Perumal, M., Moramarco, T., Sahoo, B., & Barbetta, S. (2007). A methodology for discharge estimation and rating curve development at ungauged river sites: RATING CURVE ESTIMATION AT UNGAUGED RIVER SITES. *Water Resources Research*, *43*(2). <https://doi.org/10.1029/2005WR004609>
- Robert Brakenridge, G., Cohen, S., Kettner, A. J., De Groeve, T., Nghiem, S. V., Syvitski, J. P. M., & Fekete, B. M. (2012). Calibration of satellite measurements of river discharge using a global hydrology model. *Journal of Hydrology*, *475*, 123–136. <https://doi.org/10.1016/j.jhydrol.2012.09.035>
- Sahoo, D. P., Sahoo, B., & Tiwari, M. K. (2020a). *Performance Evaluation of Remote Sensing-based High Frequent Streamflow Estimation Models at the Bramhani River Basin Outlet*. 2020, H011-0003.
- Sahoo, D. P., Sahoo, B., & Tiwari, M. K. (2020b). Copula-based probabilistic spectral algorithms for high-frequent streamflow estimation. *Remote Sensing of Environment*, *251*, 112092. <https://doi.org/10.1016/j.rse.2020.112092>
- Scherer, D., Schwatke, C., & Dettmering, D. (2020). *Estimation of River Discharge using Multi-Mission Satellite Altimetry and Optical Remote Sensing Imagery*. 15.
- Schneider, R., Godiksen, P., Rannal, H., Madsen, H., & Bauer-Gottwein, P. (2017). Application of CryoSat-2 altimetry data for river analysis and modelling. *Hydrology and Earth System Sciences*, *21*, 751–764. <https://doi.org/10.5194/hess-21-751-2017>
- Sea Level. (2022). ESA Climate Office. Retrieved August 10, 2022, from <https://climate.esa.int/en/projects/sea-level/>

- Shanlong, L., Bingfang, W., Nana, Y., Fapeng, L., Meiping, W., & Jing, W. (2010). Progress in River Runoff Monitoring by Remote Sensing. *Advances in Earth Science*, 25(8), 820. <https://doi.org/10.11867/j.issn.1001-8166.2010.08.0820>
- Shi, Z., Chen, Y., Liu, Q., & Huang, C. (2020). Discharge Estimation Using Harmonized Landsat and Sentinel-2 Product: Case Studies in the Murray Darling Basin. *Remote Sensing*, 12(17), 2810. <https://doi.org/10.3390/rs12172810>
- Sichangi, A. W., Wang, L., & Hu, Z. (2018). Estimation of River Discharge Solely from Remote-Sensing Derived Data: An Initial Study Over the Yangtze River. *Remote Sensing*, 10(9), 1385. <https://doi.org/10.3390/rs10091385>
- Sichangi, A. W., Wang, L., Yang, K., Chen, D., Wang, Z., Li, X., Zhou, J., Liu, W., & Kuria, D. (2016). Estimating continental river basin discharges using multiple remote sensing data sets. *Remote Sensing of Environment*, 179, 36–53. <https://doi.org/10.1016/j.rse.2016.03.019>
- Singh, G., Mishra, A., & Sagar, D. (2013). *SBIT JOURNAL OF SCIENCES AND TECHNOLOGY ISSN 2277-8764 VOL-2, ISSUE 1, 2013*. 4.
- Smith, L., & Pavelsky, T. (2008). Estimation of river discharge, propagation speed, and hydraulic geometry from space: Lena River, Siberia. *Water Resour. Res.*, 44. <https://doi.org/10.1029/2007WR006133>
- Soni, P., Tripathi, S., & Srivastava, R. (2021). A comparison of regionalization methods in monsoon dominated tropical river basins. *Journal of Water and Climate Change*, 12(5), 1975–1996. <https://doi.org/10.2166/wcc.2021.298>
- Sun, W. C., Ishidaira, H., & Bastola, S. (2010). Towards improving river discharge estimation in ungauged basins: Calibration of rainfall-runoff models based on satellite observations of river flow width at basin outlet. *Hydrology and Earth System Sciences*, 14(10), 2011–2022. <https://doi.org/10.5194/hess-14-2011-2010>
- Tang, Q., Gao, H., Lu, H., & Lettenmaier, D. P. (2009). Remote sensing: Hydrology. *Progress in Physical Geography: Earth and Environment*, 33(4), 490–509. <https://doi.org/10.1177/0309133309346650>
- Tarpanelli, A., Amarnath, G., Brocca, L., Massari, C., & Moramarco, T. (2017). Discharge estimation and forecasting by MODIS and altimetry data in Niger-Benue River. *Remote Sensing of Environment*, 195, 96–106. <https://doi.org/10.1016/j.rse.2017.04.015>
- Tarpanelli, A., Barbetta, S., Brocca, L., & Moramarco, T. (2013). River Discharge Estimation by Using Altimetry Data and Simplified Flood Routing Modeling. *Remote Sensing*, 5(9), 4145–4162. <https://doi.org/10.3390/rs5094145>
- Tarpanelli, A., Brocca, L., Lacava, T., Melone, F., Moramarco, T., Faruolo, M., Pergola, N., & Tramutoli, V. (2013). Toward the estimation of river discharge variations using MODIS data in ungauged basins. *Remote Sensing of Environment*, 136, 47–55. <https://doi.org/10.1016/j.rse.2013.04.010>

- Tarpanelli, A., Iodice, F., Brocca, L., Restano, M., & Benveniste, J. (2020). River Flow Monitoring by Sentinel-3 OLCI and MODIS: Comparison and Combination. *Remote Sensing*, *12*(23), 3867. <https://doi.org/10.3390/rs12233867>
- Tarpanelli, A., Santi, E., Tourian, M. J., Filippucci, P., Amarnath, G., & Brocca, L. (2019). Daily River Discharge Estimates by Merging Satellite Optical Sensors and Radar Altimetry Through Artificial Neural Network. *IEEE Transactions on Geoscience and Remote Sensing*, *57*(1), 329–341. <https://doi.org/10.1109/TGRS.2018.2854625>
- Tazioli, A. (2011). Experimental methods for river discharge measurements: Comparison among tracers and current meter. *Hydrological Sciences Journal*, *56*(7), 1314–1324. <https://doi.org/10.1080/02626667.2011.607822>
- Temini, M., Lacava, T., Tarendra, L., Tramutoli, V., Ghedira, H., & Riadh, A. (2011). A multi-temporal analysis of AMSR-E data for flood and discharge monitoring during the 2008 flood in Iowa. *Hydrological Processes*, *25*(16), 2623. <https://doi.org/10.1002/hyp.8020>
- Tourian, M. J., Schwatke, C., & Sneeuw, N. (2017). River discharge estimation at daily resolution from satellite altimetry over an entire river basin. *Journal of Hydrology*, *546*, 230–247. <https://doi.org/10.1016/j.jhydrol.2017.01.009>
- Tourian, M. J., Tarpanelli, A., Elmi, O., Qin, T., Brocca, L., Moramarco, T., & Sneeuw, N. (2016). Spatiotemporal densification of river water level time series by multimission satellite altimetry: SPATIOTEMPORAL DENSIFICATION OF ALTIMETRY OVER RIVERS. *Water Resources Research*, *52*(2), 1140–1159. <https://doi.org/10.1002/2015WR017654>
- Van Dijk, A. I. J. M., Brakenridge, G. R., Kettner, A. J., Beck, H. E., De Groeve, T., & Schellekens, J. (2016). River gauging at global scale using optical and passive microwave remote sensing. *Water Resources Research*, *52*(8), 6404–6418. <https://doi.org/10.1002/2015WR018545>
- Yang, X., Pavelsky, T. M., Allen, G. H., & Donchyts, G. (2020). RivWidthCloud: An Automated Google Earth Engine Algorithm for River Width Extraction From Remotely Sensed Imagery. *IEEE Geoscience and Remote Sensing Letters*, *17*(2), 217–221. <https://doi.org/10.1109/LGRS.2019.2920225>
- Zakharova, E. A., Kouraev, A. V., Cazenave, A., & Seyler, F. (2006). Amazon River discharge estimated from TOPEX/Poseidon altimetry. *Comptes Rendus Geoscience*, *338*(3), 188–196. <https://doi.org/10.1016/j.crte.2005.10.003>
- Zakharova, E., Nielsen, K., Kamenev, G., & Kouraev, A. (2020). River discharge estimation from radar altimetry: Assessment of satellite performance, river scales and methods. *Journal of Hydrology*, *583*, 124561. <https://doi.org/10.1016/j.jhydrol.2020.124561>
- Zebin, T., Sperrin, M., Peek, N., & Casson, A. J. (2018). Human activity recognition from inertial sensor time-series using batch normalized deep LSTM recurrent networks.



*2018 40th Annual International Conference of the IEEE Engineering in Medicine and Biology Society (EMBC)*, 1–4. <https://doi.org/10.1109/EMBC.2018.8513115>

Zhang, J., Zhu, Y., Zhang, X., Ye, M., & Yang, J. (2018). Developing a Long Short-Term Memory (LSTM) based model for predicting water table depth in agricultural areas. *Journal of Hydrology*, *561*, 918–929. <https://doi.org/10.1016/j.jhydrol.2018.04.065>

Zhu, Z., & Woodcock, C. E. (2012). Object-based cloud and cloud shadow detection in Landsat imagery. *Remote Sensing of Environment*, *118*, 83–94. <https://doi.org/10.1016/j.rse.2011.10.028>